TU Delft

Delft University of Technology

Representative volume element model of triply periodic minimal surfaces (TPMS)-based electrostrictive composites for numerical evaluation of effective properties

Singh, Diwakar; Sharma, Saurav; Kumar, Rajeev; Vaish, Rahul

DOI
10.1007/s00707-022-03404-2

Publication date
2022

Document Version
Final published version

Published in
Acta Mechanica

Citation (APA)
Singh, D., Sharma, S., Kumar, R., & Vaish, R. (2022). Representative volume element model of triply periodic minimal surfaces (TPMS)-based electrostrictive composites for numerical evaluation of effective properties. *Acta Mechanica*, *234 (2023)*(2), 355-375. https://doi.org/10.1007/s00707-022-03404-2

Important note
To cite this publication, please use the final published version (if applicable).
Please check the document version above.

Copyright
Other than for strictly personal use, it is not permitted to download, forward or distribute the text or part of it, without the consent of the author(s) and/or copyright holder(s), unless the work is under an open content license such as Creative Commons.

Takedown policy
Please contact us and provide details if you believe this document breaches copyrights.
We will remove access to the work immediately and investigate your claim.

This work is downloaded from Delft University of Technology.
For technical reasons the number of authors shown on this cover page is limited to a maximum of 10.

Green Open Access added to TU Delft Institutional Repository

'You share, we take care!' - Taverne project

https://www.openaccess.nl/en/you-share-we-take-care

Otherwise as indicated in the copyright section: the publisher is the copyright holder of this work and the author uses the Dutch legislation to make this work public.

Acta Mech
https://doi.org/10.1007/s00707-022-03404-2

ORIGINAL PAPER

Diwakar Singh · Saurav Sharma · Rajeev Kumar · Rahul Vaish

Representative volume element model of triply periodic minimal surfaces (TPMS)-based electrostrictive composites for numerical evaluation of effective properties

Received: 28 March 2022 / Revised: 22 September 2022 / Accepted: 16 October 2022
© The Author(s), under exclusive licence to Springer-Verlag GmbH Austria, part of Springer Nature 2022

Abstract A model for numerical homogenization of triply periodic minimal surfaces (TPMS) based on electrostrictive composites is presented. This electrostrictive composite consists of TPMS (a three-dimensional continuous structure) implanted in a soft non-electrostrictive matrix. A representative volume element (RVE)-based approach is used to homogenize the electrostrictive composites and determine all the effective electrostrictive, mechanical, and electrical coefficients. Finite element formulation is employed to solve the nonlinear electrostrictive constitutive equations. Special attention is paid to designing the boundary conditions that permit the fast calculation based on simulations of overall deformation-induced due to mechanical and electrical loads. Interestingly, the value of the effective electrostrictive coefficient of the composite surpasses that of the inclusion Pb $(mg_{1/3}Nb_{2/3})O_3$-$PbTO_3$-$BaTiO_3$ (PMN-PT-BT), even though the matrix is non-electrostrictive due to the additional flexibility imparted by the matrix. This electrostrictive response of TPMS-based composite is independent of the type of TPMS structures used. It is prudent to say that these composites will find their place in practical application owing to their salient features of more flexibility and high electrostrictive coefficient.

1 Introduction

The coupling of elastic and electric fields exists among many electromechanical materials such as piezoelectric [1, 2], flexoelectric [3–6], and electrostrictive [7–9]. The materials are also known as smart materials because they can respond to the change in their surrounding stimuli such as mechanical strain or electric potential. The dielectric materials with a non-centrosymmetric structure generating mechanical strain when acted upon with electric polarization and vice versa, are called piezoelectric materials (for example, ZnO and quartz). Owing to such capability piezoelectric material founds its application in actuation, sensing, and energy harvesting. While the piezoelectric effect is limited to non-centrosymmetric materials, flexoelectricity can be obtained in all dielectric materials. A mechanical strain gradient can induce sufficient polarization and vice versa in micro- and nano-dielectric material, also known as flexoelectricity. Piezoelectricity and flexoelectricity are those electromechanical phenomena where mechanical strain exhibits linear dependence on the electric field and vice-versa. However, the electrostrictive materials show a nonlinear relationship between elastic and electric field, i.e., mechanical strain depends on the square of the electric polarization and vice-versa (also known as electrostriction). Unlike piezoelectricity and flexoelectricity, electrostriction is not limited by the symmetricity and size scale of the material, respectively. Electrostriction exists in all dielectric materials at the macro-, meso-, micro-, and nanoscale. Owing to the electrostriction property, any dielectric material can generate strain in

D. Singh (✉) · S. Sharma · R. Kumar · R. Vaish
School of Engineering, Indian Institute of Technology Mandi, Himachal Pradesh, Mandi 175075, India
e-mail: d19002@students.iitmandi.ac.in

S. Sharma
Faculty of Mechanical, Maritime and Materials Engineering, Delft University of Technology, Mekelweg 2, 2628 CD Delft, The Netherlands

Published online: 02 November 2022

response to the electrical polarization [10], unlike piezoelectric materials, which require prior polling. In these electrostrictive (dielectric) materials, the displacement of ions occurs in the crystal lattice when subjected to an electric field. Positive ions move in the same direction, whereas negative ions move opposite to the direction of the applied electric field. The displaced ions cause the overall strain in the electrostrictive material. Electrostrictive materials find their applications both as sensors and actuators owing to their functionality of energy conversion reciprocity between mechanical energy and electrical energy. The most attractive choice of research fraternity for actuators is lead magnesium niobate, Pb ($mg_{1/3}Nb_{2/3}$)O_3-$PbTO_3$-$BaTiO_3$ (PMN-PT-BT), which is a ferroelectric ceramic [10]. Regardless of being effective and interesting materials, their applications are limited because of reasons such as low flexibility, density (causes obstruction in shape control), and large acoustic impedance. All these bottlenecks of electrostrictive materials can be addressed by designing a composite material. Electrostrictive composites find their potential applications in sensors, dampers, actuators, medical imaging. A set of nonlinear constitutive equations were put forward by Hom and Shankar [11] for electrostrictive materials, by considering that the generated strain depends on the second-order polarization term. This dependence of strain on second-order polarization term makes electrostriction a nonlinear problem. They also developed a static finite element formulation to simulate the induced strain at a higher electric field [12]. Due to the constantly growing demand for miniaturized autonomous electronic systems, research fraternities have resorted to designing electrostrictive composites [7–9]. Motivated by experimental studies [11, 13], researchers started simulating [7, 14–16] polymer-based electrostrictive composites to evaluate their overall macroscopic behavior. Despite significant research in linear micromechanics modeling of electro-mechanical composites [17–20], these models cannot be employed to determine nonlinear micromechanical effective properties of electrostrictive properties. Few researchers attempted to address the nonlinear micromechanics problem by decoupling it, i.e., evaluating effective mechanical [21–23] and effective dielectric properties [24] independently. An experimental approach was put forward by Guillot et al. [25] by measuring the strain and then using the Rayleigh–Ritz method to minimize the energy, which helped in determining three electrostrictive coefficients. After these, Li and Rao [26] presented a numerical algorithm for a micromechanical model to evaluate the effective overall behavior of electrostrictive composite. Lebrun et al. [27] have developed the empirical formula to predict the electrostrictive coefficient based on the effective dielectric constant and effective compliance coefficient of the electrostrictive polymer composite. They employed the Euler–Bernoulli vibration transmission theory to enact the electrostrictive coefficient predicting model. An incremental formulation employing the variational asymptotic method was used to develop the micromechanics model to predict the electrostrictive model [15]. Wang et al. [25] predicted the overall behavior of electrostrictive cubic single crystal properties from Berry's phase approach. A two-dimensional model without employing periodic boundary conditions in particulate composite was modelled by Diguet et al. [7] to predict the physical behavior. Electrostrictive material is embedded into non-electrostrictive material to convert the electrical energy into mechanical energy more effectively. Geometric configuration of electrostrictive material highly influences the electrostrictive composite. These geometric configuration are generally classified as: (1) particulate composite, in which the electrostrictive material is randomly dispersed in the matrix (represented by '0'), (2) fiber composite, in which electrostrictive material is embedded as fiber in matrix, represented by '1', (3) laminate composite, in which electrostrictive material is of planetary shape (represented by '2'), and (4) composites in which electrostrictive material is of continuous spatial structure embedded in the matrix (represented by '3'). Electrostrictive composites are lacking deliberate designing attempts; researchers have studied 0–3 [7] and 1–3 composites, but more work is required to investigate the optimum electrostrictive composites in various applications.

Advances in manufacturing technology have offered new kinds of cellular structures, i.e., triply periodic minimal surfaces (TPMS)-based composites that possess three-dimensional connectivity and better mechanical properties [28–30]. The mechanical properties of these cellular composites depend not only on their constituent materials but also on the topology of the unit cell. The two entwined domains are divided by an infinite sheet periodic in three mutually perpendicular directions. The salient features of these sheets are minimal area within a specified domain and the zero-mean curvature at any point [31]. Moreover, researchers have used mathematical equations to produce a different type of TPMS-based unit cell for functional grading and hybridization [32–35]. Many researchers have determined the mechanical, electrical, and thermal attributes of TPMS-based structures [36–40]. Moreover, Abueidda et al. [36, 41, 42] reported that these structures exhibit better properties as compared to their analog structure due to their better interconnectivity. Following the above work, Abueidda et al. [43] have investigated six different types of TPMS for electrical and thermal conductivity. The better interconnectivity of TPMS-based structures serves two appealing points, i.e., avoiding stress concentrations and smooth load transfer [43].

The current study focuses on numerical homogenization techniques (i.e., finite element method with periodic boundary conditions) employing the concept of RVE toward general procedure to determine all the effective properties of four different TPMS-based electrostrictive composites. For this study, matrix and TPMS structures are considered to be made up of epoxy and PMN-PT-BT, respectively. Section 2 elaborates on the process of generating different TPMS-based RVEs, some basic concepts, equations about electrostriction, numerical homogenization, periodic boundary conditions, and finite element formulation to solve nonlinear electrostrictive constitutive equations. Section 3 reports and discusses the results of the effective properties of the TPMS-based composites. Section 4 states the conclusion of this paper.

2 Numerical homogenization of TPMS-based electrostrictive composite

This section deals with the prediction of the effective properties of different TPMS-based electrostrictive composites. To achieve the formerly stated objective, different structural RVEs with varying volume fractions are generated using MSLattice software. Four different TPMS structures, i.e., Schoen IWP, Schwarz primitive, Schoen Gyroid, and Neovius, are focused upon.

2.1 Generation of TPMS-based RVE

Researchers have proposed various methods to generate coordinates that can imitate TPMS-based RVE [33, 44, 45]. However, the most accepted and uncomplicated method for TPMS-based RVE is level set equations. Moreover, these level set equations comprise the trigonometric term that represents an iso-surface $\Psi(x, y, z)$, which are plotted at an iso-value t. Two equal volume subdomains can be obtained if t selected as 0. Alteration of the value of t will give control over the volume possessed by TPMS structures. Considering the function as $\Psi^2 = t^2$, a sheet-based structure can be generated, where the thickness of sheet is controlled by parameter t. The current study focuses on four TPMS-based structures (i.e., Schoen IWP, Schwarz primitive, Schoen Gyroid and Neovius), which were obtained using the following level set equations [46, 47]:

Schoen IWP:

$$\Psi_{IWP} = (2(\cos X + \cos Y + \cos Z) - (\cos 2X + \cos 2Y + \cos 2Z))^2 = t^2, \tag{1}$$

Schwarz Primitive:

$$\Psi_P = (\cos X + \cos Y + \cos Z)^2 = t^2, \tag{2}$$

Schoen Gyroid:

$$\Psi_G = (\sin X \cos Y + \sin Y \cos Z + \sin Z \cos X)^2 = t^2, \tag{3}$$

Neovius:

$$\Psi_N = (3\cos X + \cos Y + \cos Z + 4\cos X \cos Z \cos Y)^2 = t^2, \tag{4}$$

where $X = 2\pi\xi x$, $Y = 2\pi\psi y$, and $Z = 2\pi\zeta z$, ξ, ψ, and ζ are the constants associated with the size of RVE in the mutually orthogonal directions. In the present study, a software MSLattice is used to generate structures of Schoen IWP, Schwarz primitive, Schoen Gyroid, and Neovius structures as shown in Figs. 1a–d, respectively. For performing the finite element analysis, these structures should be saved in STereoLithography (STL) format and then, these structures are surrounded by a unit cube to form RVEs of Schoen IWP, Schwarz primitive, Schoen Gyroid, and Neovius as shown in Figs. 2a–d, respectively.

2.2 Electrostriction and electrostrictive composites

Coupled electrostrictive problems are of two kinds, firstly in which electric field induces distributed force due to the generation of Maxwell stress, which is present in both conductors and insulators and conventionally also known as electrostriction. The generated stress depends on the second-order term of the electric field. However, there is also a second kind of coupling that occurs only in dielectrics owing to their constitutive nature, which states that induced strain depends on the second order of polarization, while mechanical stress also changes

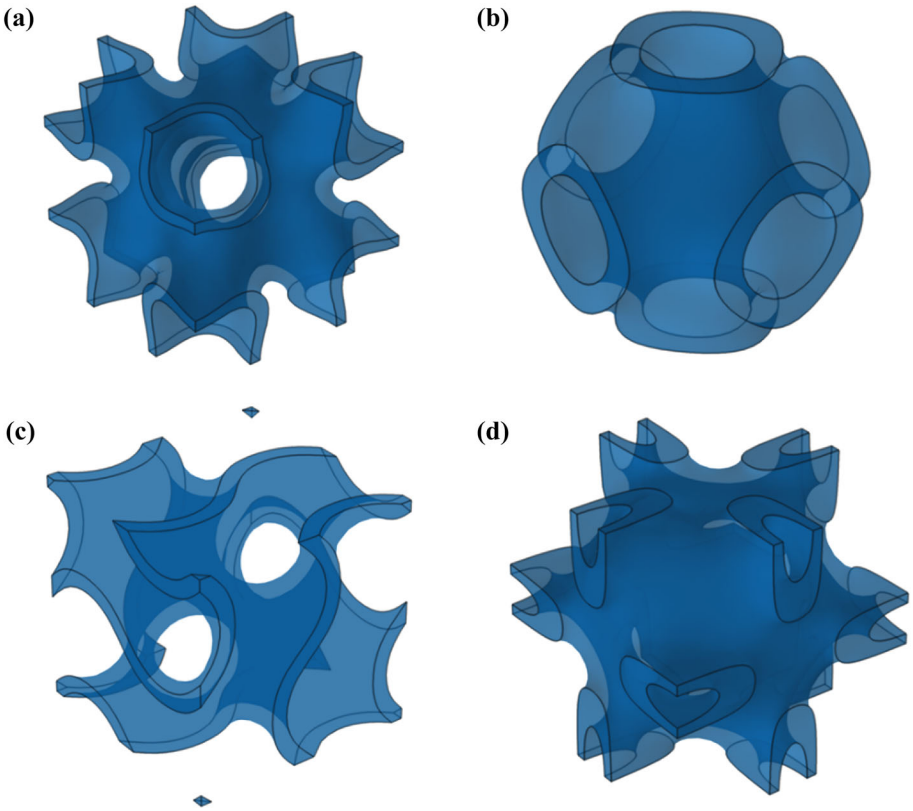

Fig. 1 Models of TPMS structures **a** Schoen IWP, **b** Schwarz primitive, **c** Schoen Gyroid, and **d** Neovius

polarization [12]. Unlike piezoelectricity, the coupling is nonlinear in electrostriction due to the dependence of induced strain on the second order of polarization. Therefore, the behavior of the electrostrictive materials can be stated with the help of constitutive equations relating electric displacement $\boldsymbol{D}$, and stress $\boldsymbol{T}$ to strain $\boldsymbol{\varepsilon}$ and electric field $\boldsymbol{E}$, which can be written as [48]

$$\boldsymbol{\varepsilon}_{ij} = \boldsymbol{S}_{ijkl}\boldsymbol{T}_{kl} + \boldsymbol{Q}_{ijlm}\boldsymbol{D}_l\boldsymbol{D}_m, \tag{5}$$

$$\boldsymbol{E}_i = -2\boldsymbol{Q}_{klji}\boldsymbol{D}_j\boldsymbol{T}_{kl} + \boldsymbol{\beta}^t_{ij}\boldsymbol{D}_j, \tag{6}$$

where $\boldsymbol{S}_{ijkl}$ is a fourth-order elastic compliance tensor, $\boldsymbol{\beta}^t_{ij}$ is the second-order dielectric impermeability constant matrix, the superscript t stands for transpose, and $\boldsymbol{Q}_{ijlm}$ is the fourth-order electrostrictive constant tensor, which can also be defined as:

$$2\boldsymbol{Q}_{ijkl} = \frac{\partial^2 \boldsymbol{\varepsilon}_{ij}}{\partial \boldsymbol{D}_k \partial \boldsymbol{D}_l} = -\frac{\partial^2 \boldsymbol{E}_l}{\partial \boldsymbol{T}_{ij} \partial \boldsymbol{D}_k}. \tag{7}$$

For electric field $\boldsymbol{E} > 0.6$ MV/m, polarization starts saturating. Inspired by Devonshire's theory [49] and Suo's adaptation [50], Hom and Shankar [11] proposed a model for relaxor ferroelectric based on a few assumptions such as (a) induced strain is proportional to the second order of polarization, (b) temperature and pressure do not influence the elastic modulus of the crystal and (c) a hyperbolic tangent function can be used to describe the stress-free dielectric behavior:

$$|\boldsymbol{P}| = P_s \tanh(k|\boldsymbol{E}|), \tag{8}$$

where P_s is the saturated value of polarization at the very high electric field, k is the material constant, and $|\boldsymbol{P}|$ and $|\boldsymbol{E}|$ are the magnitude of the polarization and electric field. It can be considered that $\boldsymbol{P} \approx \boldsymbol{D}$ because of

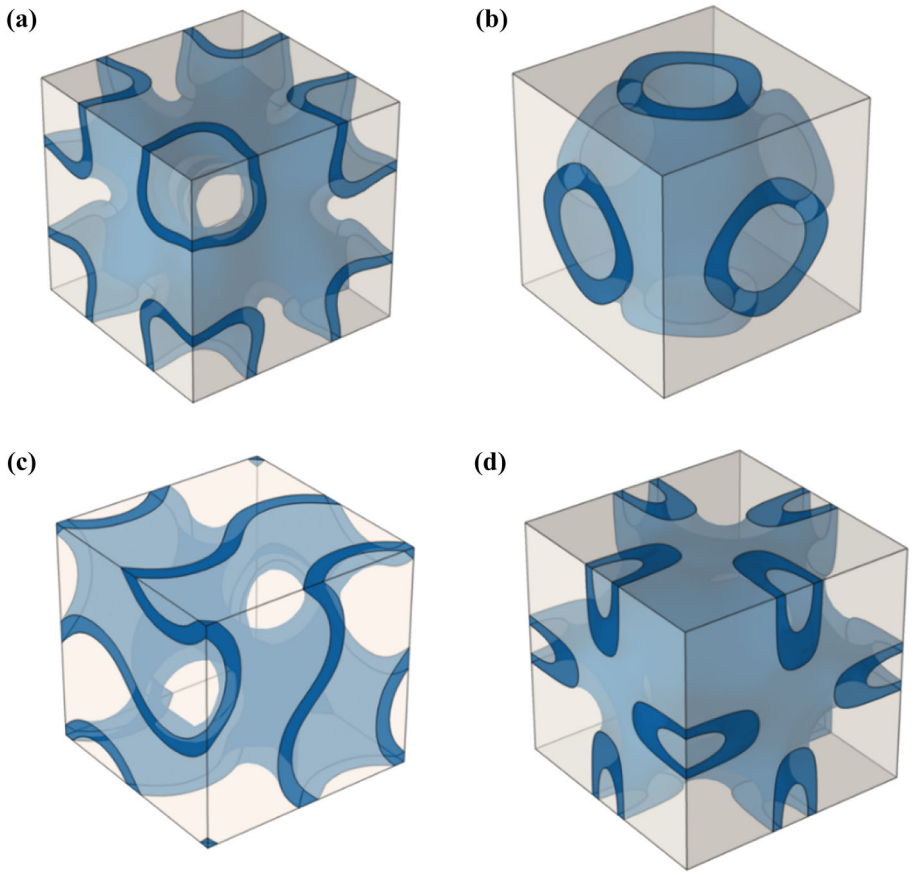

Fig. 2 RVEs of TPMS structures **a** Schoen IWP, **b** Schwarz primitive, **c** Schoen Gyroid, and **d** Neovius

the very large dielectric permittivity of ceramic, where $\boldsymbol{P}$ is polarization and $\boldsymbol{D}$ is electric displacement [48]. Therefore, Eqs. (5) and (6) can be written in condensed form as

$$\{\boldsymbol{\varepsilon}\} = [\boldsymbol{S}]\{\boldsymbol{T}\} + [\boldsymbol{g}([Q], \boldsymbol{D})]^{\mathrm{t}}\{\boldsymbol{D}\}, \tag{9}$$

$$\{\boldsymbol{E}\} = -2[\boldsymbol{g}([Q], \boldsymbol{D})]\{\boldsymbol{T}\} + \left[\boldsymbol{\beta}^{\mathrm{t}}(k, P_{\mathrm{s}}, \boldsymbol{D})\right]\{\boldsymbol{D}\}, \tag{10}$$

where

$$[\boldsymbol{g}] = \begin{bmatrix} Q_{11}D_1 & Q_{12}D_1 & Q_{12}D_1 & 0 & (Q_{11}-Q_{12})D_3 & (Q_{11}-Q_{12})D_2 \\ Q_{12}D_2 & Q_{11}D_2 & Q_{12}D_2 & (Q_{11}-Q_{12})D_3 & 0 & (Q_{11}-Q_{12})D_1 \\ Q_{11}D_3 & Q_{12}D_3 & Q_{11}D_3 & (Q_{11}-Q_{12})D_2 & (Q_{11}-Q_{12})D_1 & 0 \end{bmatrix}, \tag{11}$$

$$\left[\boldsymbol{\beta}^{\mathrm{t}}\right] = \begin{bmatrix} \frac{1}{k|\boldsymbol{D}|}arctanh\left(\frac{|\boldsymbol{D}|}{P_s}\right) & 0 & 0 \\ 0 & \frac{1}{k|\boldsymbol{D}|}arctanh\left(\frac{|\boldsymbol{D}|}{P_s}\right) & 0 \\ 0 & 0 & \frac{1}{k|\boldsymbol{D}|}arctanh\left(\frac{|\boldsymbol{D}|}{P_s}\right) \end{bmatrix}, \tag{12}$$

$$k = \frac{1}{P_s(\beta_{33})_{D=0}}, \tag{13}$$

where Q_{ij} is the electrostrictive coefficient. There are only 10 independent coefficients including compliance coefficients, electrostrictive coefficients, and impermeability coefficients for transversely isotropic electrostrictive solid. Hence, Eqs. (9) and (10) can be written in matrix form as:

$$\begin{Bmatrix} \overline{\varepsilon}_{11} \\ \overline{\varepsilon}_{22} \\ \overline{\varepsilon}_{33} \\ \overline{\varepsilon}_{23} \\ \overline{\varepsilon}_{31} \\ \overline{\varepsilon}_{12} \\ \overline{E}_1 \\ \overline{E}_2 \\ \overline{E}_3 \end{Bmatrix} = \begin{bmatrix} S_{11}^{\text{eff}} & S_{12}^{\text{eff}} & S_{13}^{\text{eff}} & 0 & 0 & 0 & Q_{11}^{\text{eff}}\overline{D}_1 & Q_{12}^{\text{eff}}\overline{D}_2 & Q_{12}^{\text{eff}}\overline{D}_3 \\ S_{12}^{\text{eff}} & S_{11}^{\text{eff}} & S_{13}^{\text{eff}} & 0 & 0 & 0 & Q_{12}^{\text{eff}}\overline{D}_1 & Q_{11}^{\text{eff}}\overline{D}_2 & Q_{12}^{\text{eff}}\overline{D}_3 \\ S_{13}^{\text{eff}} & S_{13}^{\text{eff}} & S_{33}^{\text{eff}} & 0 & 0 & 0 & Q_{12}^{\text{eff}}\overline{D}_1 & Q_{12}^{\text{eff}}\overline{D}_2 & Q_{11}^{\text{eff}}\overline{D}_3 \\ 0 & 0 & 0 & S_{44}^{\text{eff}} & 0 & 0 & 0 & \left(Q_{11}^{\text{eff}} - Q_{12}^{\text{eff}}\right)\overline{D}_3 & \left(Q_{11}^{\text{eff}} - Q_{12}^{\text{eff}}\right)\overline{D}_2 \\ 0 & 0 & 0 & 0 & S_{44}^{\text{eff}} & 0 & \left(Q_{11}^{\text{eff}} - Q_{12}^{\text{eff}}\right)\overline{D}_3 & 0 & \left(Q_{11}^{\text{eff}} - Q_{12}^{\text{eff}}\right)\overline{D}_1 \\ 0 & 0 & 0 & 0 & 0 & S_{66}^{\text{eff}} & \left(Q_{11}^{\text{eff}} - Q_{12}^{\text{eff}}\right)\overline{D}_2 & \left(Q_{11}^{\text{eff}} - Q_{12}^{\text{eff}}\right)\overline{D}_1 & 0 \\ -2Q_{11}^{\text{eff}} & -2Q_{12}^{\text{eff}} & -2Q_{12}^{\text{eff}} & 0 & -2\left(Q_{11}^{\text{eff}} - Q_{12}^{\text{eff}}\right) & -2\left(Q_{11}^{\text{eff}} - Q_{12}^{\text{eff}}\right) & \beta_{11}^{\text{eff}} & 0 & 0 \\ -2Q_{12}^{\text{eff}} & -2Q_{11}^{\text{eff}} & -2Q_{12}^{\text{eff}} & -2\left(Q_{11}^{\text{eff}} - Q_{12}^{\text{eff}}\right) & 0 & -2\left(Q_{11}^{\text{eff}} - Q_{12}^{\text{eff}}\right) & 0 & \beta_{22}^{\text{eff}} & 0 \\ -2Q_{12}^{\text{eff}} & -2Q_{12}^{\text{eff}} & -2Q_{11}^{\text{eff}} & -2\left(Q_{11}^{\text{eff}} - Q_{12}^{\text{eff}}\right) & -2\left(Q_{11}^{\text{eff}} - Q_{12}^{\text{eff}}\right) & 0 & 0 & 0 & \beta_{33}^{\text{eff}} \end{bmatrix} \begin{Bmatrix} \overline{T}_{11} \\ \overline{T}_{22} \\ \overline{T}_{33} \\ \overline{T}_{23} \\ \overline{T}_{31} \\ \overline{T}_{12} \\ \overline{D}_1 \\ \overline{D}_2 \\ \overline{D}_3 \end{Bmatrix}. \tag{14}$$

2.3 Periodic boundary conditions for the representative volume element

Any general structure under consideration is considered as a large-scale or macroscopic structure, whereas the mechanical and physical properties of constituent materials are known as microscopic structures. The most adaptive tool for the modeling of composites is homogenization, in which an equivalent medium is obtained such that the strain energies stored in the original composite and equivalent medium are equal. Homogenization is the best tool to speed up the modeling process of composites, i.e., for the discretization and computational simulation. Different homogenization techniques have been used before as discussed in the introduction. In the current study, finite element method is used to evaluate the effective properties of TPMS-based electrostrictive composite.

A representative volume element (RVE) can be periodically organized in three mutually perpendicular directions to form the original composite. Therefore, the RVE should be subjected to periodic boundary conditions to ascertain that each RVE is undergoing the same deformation and there is no overlapping or separation between the adjacent RVEs while deforming. Suquet [51] had reported the periodic boundary condition in Cartesian coordinates over RVE surfaces as

$$u_i = \overline{\varepsilon}_{ij} x_j + v_i, \tag{15}$$

where $\overline{\varepsilon}_{ij}$ is the average strain and v_i is a local fluctuation of the displacement component, which is unknown and depends on the applied load. The above general Equation (15) can be used to write the equations which explicitly show displacement on the opposite surfaces of RVE as:

$$u_i^{K^+} = \overline{\varepsilon}_{ij} x_j^{K^+} + v_i^{K^+}, \tag{16}$$

$$u_i^{K^-} = \overline{\varepsilon}_{ij} x_j^{K^-} + v_i^{K^-}, \tag{17}$$

where the superscripts K^+ and K^- represent the opposite surfaces of RVE in positive and negative x_j directions, respectively. As shown in Fig. 3, these K^+ and K^- indices represent the opposite surfaces such as A^+/A^-, B^+/B^-, and C^+/C^- in the x_1, x_2, and x_3 directions.

Moreover, the value of local fluctuations (i.e., $v_i^{K^+}$ and $v_i^{K^-}$) is approximately the same on the opposite surfaces of RVE; therefore, subtracting Eqs. (16) and (17) will result in

$$u_i^{K^+} - u_i^{K^-} = \overline{\varepsilon}_{ij}\left(x_j^{K^+} - x_j^{K^-}\right). \tag{18}$$

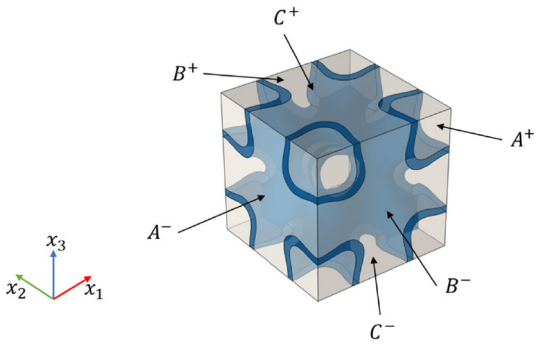

Fig. 3 Pictorial representation of the representative volume element along with notations for its surfaces

It is considered that the mean mechanical and electrical properties of the RVE are equal to the mean properties of the electrostrictive composites, which can be written as:

$$\overline{\varepsilon}_{ij} = \frac{1}{V}\int_V \varepsilon_{ij}\mathrm{d}V,\ \overline{T}_{ij} = \frac{1}{V}\int_V T_{ij}\mathrm{d}V, \tag{19}$$

$$\overline{E}_i = \frac{1}{V}\int_V E_i\mathrm{d}V, \text{ and } \overline{D}_i = \frac{1}{V}\int_V D_i\mathrm{d}V. \tag{20}$$

2.4 Finite element formulation

Consider a domain Ω, surrounded by a closed surface Γ in static equilibrium under the body force $\boldsymbol{f}^{\mathrm{b}}$, and surface traction $\boldsymbol{t}$. Therefore, from the balance of linear moment,

$$\int_\Omega \boldsymbol{f}^{\mathrm{b}}\mathrm{d}\Omega + \int_\Gamma \boldsymbol{t}^{(\mathrm{n})}\mathrm{d}\Gamma = 0, \tag{21}$$

where surface traction in tensor notation is $\boldsymbol{t}^{(\mathrm{n})} = \boldsymbol{n}.\boldsymbol{T}$, substituting $\boldsymbol{t}^{(\mathrm{n})}$ and using the Green–Gauss divergence theorem,

$$\int_\Gamma \boldsymbol{n}.\boldsymbol{T}\mathrm{d}\Gamma = \int_\Omega \nabla.\boldsymbol{T}\mathrm{d}\Omega. \tag{22}$$

Substituting Eq. (22) into Eq. (21), the obtained expression is as follows:

$$\int_\Omega \left(\nabla.\boldsymbol{T} + \boldsymbol{f}^{\mathrm{b}}\right)\mathrm{d}\Omega = 0. \tag{23}$$

Therefore, the balance of the linear moment equation at every point of a domain can be written as:

$$\nabla.\boldsymbol{T} + \boldsymbol{f}^{\mathrm{b}} = 0. \tag{24}$$

For the dielectric solid, Gauss law states that the net electric flux is equal to the total charge enclosed by the volume Ω divided by the permittivity of free space b_0; hence, this statement can be expressed as

$$\int_\Gamma \boldsymbol{n}.\boldsymbol{E}\mathrm{d}\Gamma = \frac{1}{b_0}\int_\Omega \left(q^* - \nabla.\boldsymbol{P}\right)d\Omega, \tag{25}$$

where q^* is the volumetric charge density, $\boldsymbol{n}$ is the unit normal outward vector, and $\boldsymbol{P}$ is polarization. The polarization $\boldsymbol{P}$ induces the volumetric charge density represented by the second term on right-hand side of Eq. (25). Using the Green–Gauss divergence theorem, Eq. (25) can be rewritten as:

$$b_0\int_\Omega \nabla.\boldsymbol{E}\mathrm{d}\Omega + \int_\Omega \nabla.\boldsymbol{P}\mathrm{d}\Omega = \int_\Omega q^*\mathrm{d}\Omega, \tag{26}$$

$$\int_\Omega \nabla.(b_0\boldsymbol{E} + \boldsymbol{P})\mathrm{d}\Omega = \int_\Omega q^*\mathrm{d}\Omega, \tag{27}$$

$$\int_{\Omega} \nabla.\boldsymbol{D} d\Omega - \int_{\Omega} q^* \mathrm{d}\Omega = 0. \tag{28}$$

Therefore, the electrostatic equilibrium at every point of a domain can be written as:

$$\nabla.\boldsymbol{D} - q^* = 0. \tag{29}$$

To find out stress $\boldsymbol{T}$ and dielectric field $\boldsymbol{D}$ for the electrostrictive material, Eqs. (9) and (10) must be inverted; therefore, on inverting Eq. (9), the obtained equation is as follows:

$$\boldsymbol{T} = [\boldsymbol{S}]^{-1}\boldsymbol{\varepsilon} - [\boldsymbol{S}]^{-1}[\boldsymbol{g}([Q], \boldsymbol{D})]^{\mathrm{t}}\boldsymbol{D}, \tag{30}$$

and on inverting Eq. (10) and substituting $\boldsymbol{T}$ from Eq. (30) in it, the obtained equation is as follows:

$$\boldsymbol{E} = -2[\boldsymbol{g}([Q], \boldsymbol{D})][\boldsymbol{S}]^{-1}\boldsymbol{\varepsilon} + \left(2[\boldsymbol{g}([Q], \boldsymbol{D})] \times [\boldsymbol{S}]^{-1}[\boldsymbol{g}([Q], \boldsymbol{D})]^{\mathrm{t}} + \left[\boldsymbol{\beta}^{\mathrm{t}}(k, P_s, \boldsymbol{D})\right]\right)\boldsymbol{D}. \tag{31}$$

However, Eqs. (30) and (31) can be concatenated as:

$$\boldsymbol{T} = \left[\boldsymbol{C}^{\mathrm{E}}(k, P_s, [Q], \boldsymbol{D})\right]\boldsymbol{\varepsilon} - [\boldsymbol{e}(k, P_s, [Q], \boldsymbol{D})]^{\mathrm{t}}\boldsymbol{E}, \tag{32}$$

$$\boldsymbol{D} = 2[\boldsymbol{e}(k, P_s, [Q], \boldsymbol{D})]\boldsymbol{\varepsilon} + \left[\boldsymbol{\rho}^{\mathrm{S}}(k, P_s, [Q], \boldsymbol{D})\right]\boldsymbol{E}, \tag{33}$$

where

$$\left[\boldsymbol{\rho}^{\mathrm{S}}(k, P_s, [Q], \boldsymbol{D})\right] = \left(\left[\boldsymbol{\beta}^{\mathrm{t}}(k, P_s, \boldsymbol{D})\right] + 2[\boldsymbol{g}([Q], \boldsymbol{D})][\boldsymbol{S}]^{-1}[\boldsymbol{g}([Q], \boldsymbol{D})]^{\mathrm{t}}\right)^{-1}, \tag{34}$$

$$[\boldsymbol{e}(k, P_s, [Q], \boldsymbol{D})] = \left[\boldsymbol{\rho}^{\mathrm{S}}(k, P_s, [Q], \boldsymbol{D})\right][\boldsymbol{g}([Q], \boldsymbol{D})][\boldsymbol{S}]^{-1}, \tag{35}$$

$$\left[\boldsymbol{C}^{\mathrm{E}}(k, P_s, [Q], \boldsymbol{D})\right] = [\boldsymbol{S}]^{-1} - 2[\boldsymbol{S}]^{-1}[\boldsymbol{g}([Q], \boldsymbol{D})]^{\mathrm{t}}\left[\boldsymbol{\rho}^{\mathrm{S}}(k, P_s, [Q], \boldsymbol{D})\right][\boldsymbol{g}([Q], \boldsymbol{D})][\boldsymbol{S}]^{-1}. \tag{36}$$

In the current study domain, Ω of RVE of the electrostrictive composite is discretized with four noded tetrahedral elements. Three mechanical degrees of freedom (i.e., one displacement degree of freedom in x_1, x_2, and x_3 directions, respectively) and one electrical degree of freedom (i.e., electric potential) are considered at each node of the element. The approximate elemental displacement function inside any element can be defined as:

$$\begin{Bmatrix} u^* \\ v^* \\ w^* \end{Bmatrix} = \sum_{i=1}^{4} \begin{bmatrix} N_i & 0 & 0 \\ 0 & N_i & 0 \\ 0 & 0 & N_i \end{bmatrix} \begin{Bmatrix} u_i \\ v_i \\ w_i \end{Bmatrix}, \tag{37}$$

$$\{\overline{\boldsymbol{u}}\}_{\mathrm{e}} = [\boldsymbol{N}_{\overline{\mathrm{u}}}]_{\mathrm{e}}\{\boldsymbol{q}\}_{\mathrm{e}}, \tag{38}$$

where N_i is the shape function, mentioned in Annexure A, u_i, v_i and w_i are the nodal displacements in x_1, x_2, and x_3 directions, respectively. Subscript 'e' represents elemental and $\{\boldsymbol{q}\}_{\mathrm{e}}$ is the elemental nodal displacement vector. The elemental strain can be obtained by partially differentiating the elemental nodal vector once, which is

$$\{\boldsymbol{\varepsilon}\}_{\mathrm{e}} = \begin{Bmatrix} \varepsilon_{11} \\ \varepsilon_{22} \\ \varepsilon_{33} \\ \varepsilon_{23} \\ \varepsilon_{13} \\ \varepsilon_{12} \end{Bmatrix}_{\mathrm{e}} = \begin{Bmatrix} \frac{\partial u^*}{\partial x_1} \\ \frac{\partial v^*}{\partial x_2} \\ \frac{\partial w^*}{\partial x_3} \\ \frac{\partial w^*}{\partial x_2} + \frac{\partial v^*}{\partial x_3} \\ \frac{\partial u^*}{\partial x_3} + \frac{\partial w^*}{\partial x_1} \\ \frac{\partial u^*}{\partial x_2} + \frac{\partial v^*}{\partial x_1} \end{Bmatrix}_{\mathrm{e}}, \tag{39}$$

$$\{\boldsymbol{\varepsilon}\}_{\mathrm{e}} = [\boldsymbol{B}]_{\mathrm{e}}\{\boldsymbol{q}\}_{\mathrm{e}}, \tag{40}$$

where $\{\boldsymbol{\varepsilon}\}_{\mathrm{e}}$ is the elemental strain vector, and $[\boldsymbol{B}]_{\mathrm{e}}$ is the elemental strain displacement matrix, which is given in Appendix A. The approximate electric potential function $\varnothing^*$ inside an element is

$$\varnothing^* = [N_1\ N_2\ N_3\ N_4]\begin{Bmatrix}\varnothing_1\\ \varnothing_2\\ \varnothing_3\\ \varnothing_4\end{Bmatrix}, \tag{41}$$

$$\varnothing^*_{\mathrm{e}} = [\boldsymbol{N}_{\overline{\varnothing}}]_{\mathrm{e}}\{\boldsymbol{\Phi}\}_{\mathrm{e}}, \tag{42}$$

where $\varnothing_i$, $i = 1$ to 4, is the nodal electric potential in an element. The elemental electric field can be defined as:

$$\{\boldsymbol{E}\}_{\mathrm{e}} = -\left[\boldsymbol{B}_{\phi}\right]_{\mathrm{e}}\{\boldsymbol{\Phi}\}_{\mathrm{e}}, \tag{43}$$

where the electric field and electric potential matrix $\left[\boldsymbol{B}_{\phi}\right]_{\mathrm{e}}$ are mentioned in Annexure A. As the current study is a nonlinear problem, it employs the principle of virtual work. The small arbitrary perturbation of real displacements u_i and electric potential ϕ is δu_i and $\delta\varnothing$, respectively. Hence, the weak formulation of Eqs. (24) and (29) can be given by expression for virtual work done of electrostrictive system, which is

$$\int_{\Omega}\left(T_{ij,j} + f_i^{\mathrm{b}}\right)\delta u_i \mathrm{d}\Omega + \int_{\Omega}\left(D_{i,i} - q^*\right)\delta\phi \mathrm{d}\Omega = 0, \tag{44}$$

$$\int_{\Omega} T_{ij,j}\delta u_i \mathrm{d}\Omega + \int_{\Omega} f_i^{\mathrm{b}}\delta u_i \mathrm{d}\Omega + \int_{\Omega} D_{i,i}\delta\phi \mathrm{d}\Omega - \int_{\Omega} q^*\delta\phi \mathrm{d}\Omega = 0. \tag{45}$$

The obtained equation after applying integration by parts and the Green–Gauss divergence theorem to Eq. (45) is as follows:

$$-\int_{\Omega} T_{ij}\delta u_{i,j}\mathrm{d}\Omega + \int_{\Gamma} T_{ij}n_j\delta u_i \mathrm{d}\Gamma + \int_{\Omega} f_i^{\mathrm{b}}\delta u_i \mathrm{d}\Omega - \int_{\Omega} D_i\delta\phi_{,i}\mathrm{d}\Omega + \int_{\Gamma} D_i n_i\delta\phi \mathrm{d}\Gamma - \int_{\Omega} q^*\delta\phi \mathrm{d}\Omega = 0, \tag{46}$$

$$\int_{\Omega} T_{ij}\delta\varepsilon_{ij}\mathrm{d}\Omega - \int_{\Omega} D_i\delta E_i \mathrm{d}\Omega = \int_{\Gamma} T_{ij}n_j\delta u_i \mathrm{d}\Gamma + \int_{\Omega} f_i^{\mathrm{b}}\delta u_i \mathrm{d}\Omega \int_{\Gamma} D_i n_i\delta\phi \mathrm{d}\Gamma - \int_{\Omega} q^*\delta\phi \mathrm{d}\Omega. \tag{47}$$

The terms on the left-hand side of Eq. (47) represent the internal work done, whereas all the terms on the right-hand side of Eq. (47) refer to the external work done. The principle of virtual work states that the system is in equilibrium if and only if the internal work done and external work done for every virtual displacement and virtual electric potential field are equal. Neglecting the body force f_i^{b} and volumetric charge density q^*, Eq. (47) can be rewritten as follows:

$$-\int_{\Omega}\left(T_{ij}\delta B_{ij} - D_i\delta E_i\right)\mathrm{d}\Omega + \int_{\Gamma}\left(\delta u_i T_{ij}n_j + \delta\phi D_i n_i\right)\mathrm{d}\Gamma = 0, \tag{48}$$

$$\int_{\Omega}\begin{Bmatrix}\delta\varepsilon_{ij}\\ -\delta E_i\end{Bmatrix}^{\mathrm{t}}\begin{Bmatrix}T_{ij}\\ D_i\end{Bmatrix}\mathrm{d}\Omega - \int_{\Gamma}\begin{Bmatrix}\delta u\\ \delta\varnothing\end{Bmatrix}^{\mathrm{t}}\begin{Bmatrix}f_i\\ q\end{Bmatrix}\mathrm{d}\Gamma = 0, \tag{49}$$

where $f_i = T_{ij}n_j$ and $q^* = D_i n_i$ are the forces and charge density acting on surface Γ, respectively. After applying the finite element discretization, Eq. (49) can be rewritten as:

$$\sum_{e=1}^{m}\int_{\Omega_e}\begin{Bmatrix}\delta\{\boldsymbol{\varepsilon}\}_e\\ -\delta\{\boldsymbol{E}\}_e\end{Bmatrix}^{\mathrm{t}}\begin{Bmatrix}\{\boldsymbol{T}\}_e\\ \{\boldsymbol{D}\}_e\end{Bmatrix}\mathrm{d}\Omega_e - \sum_{e=1}^{n}\int_{\Gamma_e}\begin{Bmatrix}\delta\{\boldsymbol{q}\}_e\\ \delta\{\boldsymbol{\Phi}\}_e\end{Bmatrix}^{\mathrm{t}}\begin{Bmatrix}[\boldsymbol{N}_{\overline{\mathrm{u}}}]_e^{\mathrm{t}}\{\boldsymbol{f}\}_e\\ -\left[\boldsymbol{N}_{\phi}\right]_e^{\mathrm{t}}\{\boldsymbol{q}\}_e\end{Bmatrix}\mathrm{d}\Gamma_e = 0. \tag{50}$$

On substituting $\{\boldsymbol{\varepsilon}\}$, and $\{\boldsymbol{E}\}$ from Eqs. (40) and (43) in Eq. (50), the obtained equation is as follows:

$$\sum_{e=1}^{m}\int_{\Omega_e}\begin{Bmatrix}\delta[\boldsymbol{B}]_e\{\boldsymbol{q}\}_e\\ -\delta\left[\boldsymbol{B}_{\phi}\right]_e\{\boldsymbol{\Phi}\}_e\end{Bmatrix}^{\mathrm{t}}\begin{Bmatrix}\{\boldsymbol{T}\}_e\\ \{\boldsymbol{D}\}_e\end{Bmatrix}\mathrm{d}\Omega_e - \sum_{e=1}^{n}\int_{\Gamma_e}\begin{Bmatrix}\delta\{\boldsymbol{q}\}_e\\ \delta\{\boldsymbol{\Phi}\}_e\end{Bmatrix}^{\mathrm{t}}\begin{Bmatrix}[\boldsymbol{N}_{\overline{\mathrm{u}}}]_e^{\mathrm{t}}\{\boldsymbol{f}\}_e\\ -\left[\boldsymbol{N}_{\phi}\right]_e^{\mathrm{t}}\{\boldsymbol{q}\}_e\end{Bmatrix}\mathrm{d}\Gamma_e = 0, \tag{51}$$

$$\sum_{e=1}^{m}\int_{\Omega_e}\left\{\delta\{\boldsymbol{q}\}_e^{\mathrm{t}}\delta\{\boldsymbol{\Phi}\}_e^{\mathrm{t}}\right\}\begin{bmatrix}[\boldsymbol{B}]_e^{\mathrm{t}} & 0\\ 0 & \left[\boldsymbol{B}_{\phi}\right]_e^{\mathrm{t}}\end{bmatrix}\begin{Bmatrix}\{\boldsymbol{T}\}_e\\ \{\boldsymbol{D}\}_e\end{Bmatrix}\mathrm{d}\Omega_e - \sum_{e=1}^{n}\int_{\Gamma_e}\begin{Bmatrix}\delta\{\boldsymbol{q}\}_e\\ \delta\{\boldsymbol{\Phi}\}_e\end{Bmatrix}^{\mathrm{t}}\begin{Bmatrix}[\boldsymbol{N}_{\overline{\mathrm{u}}}]_e^{\mathrm{t}}\{\boldsymbol{f}\}_e\\ -\left[\boldsymbol{N}_{\phi}\right]_e^{\mathrm{t}}\{\boldsymbol{q}\}_e\end{Bmatrix}\mathrm{d}\Gamma_e = 0. \tag{52}$$

Substituting $\{\boldsymbol{T}\}$, and $\{\boldsymbol{D}\}$ from Eqs. (32) and (33) into Eq. (52), the obtained equation is as follows:

$$\sum_{e=1}^{m}\int_{\Omega_e}\left\{\delta\{\boldsymbol{q}\}_e^{\mathrm{t}}\delta\{\boldsymbol{\Phi}\}_e^{\mathrm{t}}\right\}\begin{bmatrix}[\boldsymbol{B}]_e^{\mathrm{t}} & 0\\ 0 & [\boldsymbol{B}_\phi]_e^{\mathrm{t}}\end{bmatrix}\begin{bmatrix}[\boldsymbol{C}^{\mathrm{E}}(k,P_{\mathrm{s}},[Q],\boldsymbol{D})]_e & -[\boldsymbol{e}(k,P_{\mathrm{s}},[Q],\boldsymbol{D})]_e^{\mathrm{t}}\\ [2\boldsymbol{e}(k,P_s,[Q],\boldsymbol{D})]_e & [\boldsymbol{\varepsilon}^{\mathrm{S}}(k,P_{\mathrm{s}},[Q],\boldsymbol{D})]_e\end{bmatrix}\begin{bmatrix}[\boldsymbol{B}]_e & 0\\ 0 & -[\boldsymbol{B}_\phi]_e\end{bmatrix}\begin{Bmatrix}\{\boldsymbol{q}\}_e\\ \{\boldsymbol{\Phi}\}_e\end{Bmatrix}\mathrm{d}\Omega_e$$
$$-\sum_{e=1}^{n}\int_{\Gamma_e}\begin{Bmatrix}\delta\{\boldsymbol{q}\}_e\\ \delta\{\boldsymbol{\Phi}\}_e\end{Bmatrix}^{\mathrm{t}}\begin{Bmatrix}[\boldsymbol{N}_{\bar{\mathrm{u}}}]_e^{\mathrm{t}}\{\boldsymbol{f}\}_e\\ -[\boldsymbol{N}_\phi]_e^{\mathrm{t}}\{\boldsymbol{q}\}_e\end{Bmatrix}\mathrm{d}\Gamma_e=0. \tag{53}$$

The above Eq. (53) will attain condensed form, after defining the elemental elastic stiffness matrix $\left[\boldsymbol{K}_{\mathrm{uu}}\left(\boldsymbol{q}^i,\boldsymbol{\Phi}^i\right)\right]_e$ (where $\boldsymbol{q}^i$ and $\boldsymbol{\Phi}^i$ are the known solution after iteration i), the elemental electromechanical coupling matrix $\left[\boldsymbol{K}_{\mathrm{u}\mathbb{E}}\left(\boldsymbol{q}^i,\boldsymbol{\Phi}^i\right)\right]_e$, and the elemental dielectric stiffness matrix $\left[\boldsymbol{K}_{\mathbb{E}\mathbb{E}}\left(\boldsymbol{q}^i,\boldsymbol{\Phi}^i\right)\right]_e$ as:

$$\left[\boldsymbol{K}_{\mathrm{uu}}\left(\boldsymbol{q}^i,\boldsymbol{\Phi}^i\right)\right]_e=\int_{\Omega_e}[\boldsymbol{B}]_e^{\mathrm{t}}\left[\boldsymbol{C}^{\mathrm{E}}(k,P_{\mathrm{s}},[Q],\boldsymbol{D})\right]_e[\boldsymbol{B}]_{\mathrm{e}}\mathrm{d}\Omega_e, \tag{54}$$

$$\left[\boldsymbol{K}_{\mathrm{u}\mathbb{E}}\left(\boldsymbol{q}^i,\boldsymbol{\Phi}^i\right)\right]_e=\int_{\Omega_e}[\boldsymbol{B}]_e^{\mathrm{t}}[\boldsymbol{e}(k,P_s,[Q],\boldsymbol{D})]_e^{\mathrm{t}}\left[\boldsymbol{B}_\phi\right]_e\mathrm{d}\Omega_e, \tag{55}$$

$$\left[\boldsymbol{K}_{\mathbb{E}\mathbb{E}}\left(\boldsymbol{q}^i,\boldsymbol{\Phi}^i\right)\right]_e=\int_{\Omega_e}\left[\boldsymbol{B}_\phi\right]_e^{\mathrm{t}}\left[\boldsymbol{\varepsilon}^{\mathrm{S}}(k,P_s,[Q],\boldsymbol{D})\right]_e\left[\boldsymbol{B}_\phi\right]_e\mathrm{d}\Omega_e, \tag{56}$$

and the elemental mechanical excitation vector $\left\{\boldsymbol{F}\left(\boldsymbol{q}^i,\boldsymbol{\Phi}^i\right)\right\}_e$ and the elemental electrical excitation vector $\left\{\boldsymbol{Q}\left(\boldsymbol{q}^i,\boldsymbol{\Phi}^i\right)\right\}_e$ as:

$$\left\{\boldsymbol{F}\left(\boldsymbol{q}^i,\boldsymbol{\Phi}^i\right)\right\}_e=\int_{\Gamma_e}[\boldsymbol{N}_{\bar{\mathrm{u}}}]_e^{\mathrm{t}}\{\boldsymbol{f}\}_e\mathrm{d}\Gamma_e, \tag{57}$$

$$\left\{\boldsymbol{Q}\left(\boldsymbol{q}^i,\boldsymbol{\Phi}^i\right)\right\}_e=\int_{\Gamma_e}\left[\boldsymbol{N}_\phi\right]_e^{\mathrm{t}}\{\boldsymbol{q}\}_e\mathrm{d}\Gamma_e. \tag{58}$$

Hence, the condensed elemental finite element equation is as follows:

$$\left\{\delta\{\boldsymbol{q}\}_e^{\mathrm{t}}\delta\{\boldsymbol{\Phi}\}_e^{\mathrm{t}}\right\}\left(\begin{bmatrix}\left[\boldsymbol{K}_{\mathrm{uu}}\left(\boldsymbol{q}^i,\boldsymbol{\Phi}^i\right)\right]_e & \left[\boldsymbol{K}_{\mathrm{u}\mathbb{E}}\left(\boldsymbol{q}^i,\boldsymbol{\Phi}^i\right)\right]_e\\ 2\left[\boldsymbol{K}_{\mathrm{u}\mathbb{E}}\left(\boldsymbol{q}^i,\boldsymbol{\Phi}^i\right)\right]_e & -\left[\boldsymbol{K}_{\mathbb{E}\mathbb{E}}\left(\boldsymbol{q}^i,\boldsymbol{\Phi}^i\right)\right]_e\end{bmatrix}\begin{Bmatrix}\left\{\boldsymbol{q}^{i+1}\right\}_e\\ \left\{\boldsymbol{\Phi}^{i+1}\right\}_e\end{Bmatrix}-\begin{Bmatrix}\left\{\boldsymbol{F}\left(\boldsymbol{q}^i,\boldsymbol{\Phi}^i\right)\right\}_e\\ \left\{\boldsymbol{Q}\left(\boldsymbol{q}^i,\boldsymbol{\Phi}^i\right)\right\}_e\end{Bmatrix}\right)=0. \tag{59}$$

After assembly of these elemental systems of equations, global finite element equation for static analysis is obtained, which is,

$$\begin{bmatrix}\left[\boldsymbol{K}_{\mathrm{uu}}\left(\boldsymbol{q}^i,\boldsymbol{\Phi}^i\right)\right] & \left[\boldsymbol{K}_{\mathrm{u}\mathbb{E}}\left(\boldsymbol{q}^i,\boldsymbol{\Phi}^i\right)\right]\\ 2\left[\boldsymbol{K}_{\mathrm{u}\mathbb{E}}\left(\boldsymbol{q}^i,\boldsymbol{\Phi}^i\right)\right] & -\left[\boldsymbol{K}_{\mathbb{E}\mathbb{E}}\left(\boldsymbol{q}^i,\boldsymbol{\Phi}^i\right)\right]\end{bmatrix}\begin{Bmatrix}\left\{\boldsymbol{q}^{i+1}\right\}\\ \left\{\boldsymbol{\Phi}^{i+1}\right\}\end{Bmatrix}=\begin{Bmatrix}\left\{\boldsymbol{F}\left(\boldsymbol{q}^i,\boldsymbol{\Phi}^i\right)\right\}\\ \left\{\boldsymbol{Q}\left(\boldsymbol{q}^i,\boldsymbol{\Phi}^i\right)\right\}\end{Bmatrix}. \tag{60}$$

Equation (60) is a nonlinear equation as $\left[\boldsymbol{K}_{\mathrm{uu}}\left(\boldsymbol{q}^i,\boldsymbol{\Phi}^i\right)\right]$, $\left[\boldsymbol{K}_{\mathrm{u}\mathbb{E}}\left(\boldsymbol{q}^i,\boldsymbol{\Phi}^i\right)\right]$, and $\left[\boldsymbol{K}_{\mathbb{E}\mathbb{E}}\left(\boldsymbol{q}^i,\boldsymbol{\Phi}^i\right)\right]$ depends on electric displacement D, which can be observed using Eqs. (34), (35), (36), (54), (55), and (56). Therefore, to solve the global finite element Eq. (60), Newton–Raphson method is used.

2.5 Boundary condition to determine effective electrostrictive properties

To determine the effective properties of the electrostrictive composite, it is required to subject the representative volume element to periodic boundary conditions. Using Eqs. (14), a final formula can be derived for each effective property, which is also given in Table 1.

The following notations are used in Table 1 for explaining the distinct boundary conditions on the different surfaces (i.e., $\mathrm{A}^+/\mathrm{A}^-$, $\mathrm{B}^+/\mathrm{B}^-$, and $\mathrm{C}^+/\mathrm{C}^-$ in the x_1, x_2, and x_3 directions, see Fig. 3) of RVE. 0 represents the prescribed zero displacement or electric potential, $-$ represents the unprescribed value of displacement u_i of electric potential ϕ, $\overline{\phi}$ is the prescribed nonzero electric potential, and $\overline{u}_i$ represents the constraint coupling of displacement component u_1 on an opposite surface of RVE. Applying the appropriate boundary conditions to the surfaces of the representative volume element, as prescribed in Table 1, effective properties can be evaluated. Elaborated discussion to investigate effective properties is given below.

Table 1 Appropriate boundary conditions and formulas for effective electrostrictive properties

Eff. Coe	A^- u_i/ϕ	A^+ u_i/ϕ	B^- u_i/ϕ	B^+ u_i/ϕ	C^- u_i/ϕ	C^+ u_i/ϕ	Formula
S_{11}^{eff}	$0/-$	$\overline{u}_1/0$	$0/-$	$-/-$	0/0	$-/0$	$\frac{\overline{\varepsilon}_{11}}{\overline{T}_{11}}$
S_{12}^{eff}	$0/-$	$\overline{u}_1/0$	$0/-$	$-/-$	0/0	$-/0$	$\frac{\overline{\varepsilon}_{22}}{\overline{T}_{11}}$
S_{13}^{eff}	$0/-$	$\overline{u}_1/0$	$0/-$	$-/-$	0/0	$-/0$	$\frac{\overline{\varepsilon}_{33}}{\overline{T}_{11}}$
S_{33}^{eff}	$0/-$	$-/-$	$0/-$	$-/-$	0/0	$\overline{u}_3/0$	$\frac{\overline{\varepsilon}_{33}}{\overline{T}_{33}}$
S_{44}^{eff}	$\overline{u}_3/-$	$\overline{u}_3/-$	$0/-$	$-/-$	$\overline{u}_1/0$	$\overline{u}_1/0$	$\frac{\overline{\varepsilon}_{13}}{\overline{T}_{13}}$
S_{66}^{eff}	$\overline{u}_2/-$	$\overline{u}_2/-$	$\overline{u}_1/-$	$\overline{u}_1/-$	0/0	$-/0$	$\frac{\overline{\varepsilon}_{12}}{\overline{T}_{12}}$
Q_{11}^{eff}	$0/\overline{\phi}$	$-/0$	$0/-$	$-/-$	$0/-$	$-/-$	$\frac{\overline{\varepsilon}_{11}}{(\overline{D}_1)^2}$
Q_{12}^{eff}	$0/\overline{\phi}$	$-/0$	$0/-$	$-/-$	$0/-$	$-/-$	$\frac{\overline{\varepsilon}_{22}}{(\overline{D}_1)^2}$
β_{11}^{eff}	$0/\overline{\phi}$	$-/0$	$0/-$	$-/-$	$0/-$	$-/-$	$\frac{\overline{E}_1}{\overline{D}_1}$
β_{33}^{eff}	$0/-$	$-/-$	$0/-$	$-/-$	$0/\overline{\phi}$	$-/0$	$\frac{\overline{E}_3}{\overline{D}_3}$

2.5.1 Determining the effective coefficients $\boldsymbol{S_{11}^{\text{eff}}}$, $\boldsymbol{S_{12}^{\text{eff}}}$, $\boldsymbol{S_{13}^{\text{eff}}}$, *and* $\boldsymbol{S_{33}^{\text{eff}}}$

To evaluate the effective compliance coefficients S_{11}^{eff}, S_{12}^{eff}, and S_{13}^{eff}, the boundary condition is applied such that unit tensile strain is achieved in x_1 direction, whereas the RVE is allowed to shrink in other two directions (i.e., x_2, and x_3). Moreover, the zero electric potential is applied such that there is no electric displacement in any direction. Utilizing Eq. (14) and applying such boundary conditions leads to

$$\overline{\varepsilon}_{11} = S_{11}^{\text{eff}}\overline{T}_{11} + S_{12}^{\text{eff}}\overline{T}_{22} + S_{13}^{\text{eff}}\overline{T}_{33}. \tag{61}$$

Due to the applied boundary conditions, the second and third terms on the right-hand side are very small (i.e., $S_{12}^{\text{eff}}\overline{T}_{22}$, $S_{13}^{\text{eff}}\overline{T}_{33} << S_{11}^{\text{eff}}\overline{T}_{11}$); therefore, neglecting these terms, S_{11}^{eff} can be evaluated as:

$$S_{11}^{\text{eff}} = \frac{\overline{\varepsilon}_{11}}{\overline{T}_{11}}. \tag{62}$$

Similarly, using the second and third row of Eq. (14), S_{12}^{eff} and S_{13}^{eff} can be obtained as follows:

$$S_{12}^{\text{eff}} = \frac{\overline{\varepsilon}_{22}}{\overline{T}_{11}} \text{ and } S_{13}^{\text{eff}} = \frac{\overline{\varepsilon}_{33}}{\overline{T}_{11}}. \tag{63}$$

Moreover, for estimation of the coefficient S_{33}^{eff} involves analogous boundary conditions which were prescribed to evaluate S_{11}^{eff}, and only the known strain is applied in x_3 direction, whereas the RVE is allowed to shrink in other two directions (i.e., x_1, and x_2). Therefore, utilizing the third row of Eq. (14),

$$\overline{\varepsilon}_{33} = S_{13}^{\text{eff}}\overline{T}_{11} + S_{13}^{\text{eff}}\overline{T}_{22} + S_{33}^{\text{eff}}\overline{T}_{33}. \tag{64}$$

As the second and third terms on the right-hand side are very small (i.e., $S_{13}^{\text{eff}}\overline{T}_{11}$, $S_{13}^{\text{eff}}\overline{T}_{22} << S_{33}^{\text{eff}}\overline{T}_{33}$), therefore neglecting these terms, S_{33}^{eff} can be evaluated as:

$$S_{33}^{\text{eff}} = \frac{\overline{\varepsilon}_{33}}{\overline{T}_{33}}. \tag{65}$$

2.5.2 Determining the effective coefficients $S_{44}^{\mathbf{eff}}$, and $S_{66}^{\mathbf{eff}}$

To determine the coefficients S_{44}^{eff}, and S_{66}^{eff}, the pure shear state should be enforced in $x_1 - x_3$ plane and $x_1 - x_2$ plane, respectively. To obtain pure shear state, coupling constraints on two pairs of opposite surfaces should be applied. For evaluation of coefficient S_{44}^{eff}, coupling constraint for the node pairs on opposite planes C^+/C^- can be derived from Eq. (18), i.e., $u_3^{A^+} = u_3^{A^-} + \overline{\varepsilon}_{13}\left(x_1^{A^+} - x_1^{A^-}\right)$. An arbitrary value should be assigned to $\overline{\varepsilon}_{13}\left(x_1^{A^+} - x_1^{A^-}\right)$ and prescribing the analogous coupled constraints on the paired nodes of opposite surfaces A^+/A^-, thereafter constraining the rigid body motion of RVE by restricting the motion of intersecting edge of surfaces C^- and A^- in the x_1 and x_3 directions. Therefore, using the fifth row of Eq. (14), S_{44}^{eff} can be calculated as:

$$S_{44}^{\text{eff}} = \frac{\overline{\varepsilon}_{13}}{\overline{T}_{13}}. \tag{66}$$

Similarly, applying the appropriated boundary conditions as mentioned in Table 1, S_{66}^{eff} can be calculated as:

$$S_{66}^{\text{eff}} = \frac{\overline{\varepsilon}_{12}}{\overline{T}_{12}}. \tag{67}$$

2.5.3 Determining the effective electrostrictive coefficients $\boldsymbol{Q}_{11}^{\mathbf{eff}}$, and $\boldsymbol{Q}_{12}^{\mathbf{eff}}$

Evaluation of effective electrostrictive coefficients Q_{11}^{eff}, and Q_{12}^{eff} can be achieved by applying the electric field and measuring the induced strain, for which the RVE's rigid body motion should be restrained by prescribing zero normal displacements on A^-, B^-, and C^- surfaces of RVE. At the same time, the RVE must be subjected to a known electric field, which can be achieved by applying known electric potential on the surface A^-, while electrically grounding the surface A^+. Therefore, from the first row of Eq. (14),

$$\overline{\varepsilon}_{11} = S_{11}^{\text{eff}}\overline{T}_{11} + S_{12}^{\text{eff}}\overline{T}_{22} + S_{13}^{\text{eff}}\overline{T}_{33} + Q_{11}^{\text{eff}}\left(\overline{D}_1\right)^2 + Q_{11}^{\text{eff}}\left(\overline{D}_2\right)^2 + Q_{12}^{\text{eff}}\left(\overline{D}_3\right)^2. \tag{68}$$

The first, second, third, fifth, and sixth terms on the right-hand side of Eq. (65) are negligible in comparison with the fourth term on the right-hand side (i.e., $S_{11}^{\text{eff}}\overline{T}_{11}$, $S_{12}^{\text{eff}}\overline{T}_{22}$, $S_{13}^{\text{eff}}\overline{T}_{33}$, $Q_{11}^{\text{eff}}\left(\overline{D}_2\right)^2$, and $Q_{12}^{\text{eff}}\left(\overline{D}_3\right)^2 <<< Q_{11}^{\text{eff}}\left(\overline{D}_1\right)^2$). Therefore, Q_{11}^{eff} can be calculated as:

$$Q_{11}^{\text{eff}} = \frac{\overline{\varepsilon}_{11}}{\left(\overline{D}_1\right)^2}. \tag{69}$$

Similarly, employing the second row of Eq. (14), Q_{12}^{eff} can be calculated as:

$$Q_{12}^{\text{eff}} = \frac{\overline{\varepsilon}_{22}}{\left(\overline{D}_1\right)^2}. \tag{70}$$

2.5.4 Determining the effective impermeability coefficients $\boldsymbol{\beta}_{11}^{\mathbf{eff}}$ and $\boldsymbol{\beta}_{33}^{\mathbf{eff}}$

To determine the effective impermeability coefficient β_{11}^{eff}, RVE should be subjected to zero normal displacement on A^-, B^-, and C^- surfaces, while being subject to a known nonzero electric filed in x_1 direction, by applying nonzero electric potential on surface A^- and grounding A^+ surface. Therefore, using the seventh row of Eq. (14), the relation obtained is

$$\overline{E}_1 = -2Q_{11}^{\text{eff}}\overline{T}_{11} - 2Q_{12}^{\text{eff}}\overline{T}_{22} - 2Q_{12}^{\text{eff}}\overline{T}_{33} - 2\left(Q_{11}^{\text{eff}} - Q_{12}^{\text{eff}}\right)\overline{T}_{31} - 2\left(Q_{11}^{\text{eff}} - Q_{12}^{\text{eff}}\right)\overline{T}_{12} + \beta_{11}^{\text{eff}}\overline{D}_1 + \beta_{22}^{\text{eff}}\overline{D}_2 + \beta_{33}^{\text{eff}}\overline{D}_3. \tag{71}$$

When the RVE is subjected to the formerly mentioned boundary conditions, all the terms except $\beta_{11}^{\text{eff}}\overline{D}_1$ on the right-hand side are negligible (i.e., $2Q_{11}^{\text{eff}}\overline{T}_{11}, 2Q_{12}^{\text{eff}}\overline{T}_{22}, 2Q_{12}^{\text{eff}}\overline{T}_{33}, 2\left(Q_{11}^{\text{eff}} - Q_{12}^{\text{eff}}\right)\overline{T}_{31}, 2\left(Q_{11}^{\text{eff}} - Q_{12}^{\text{eff}}\right)\overline{T}_{12}$, $\beta_{22}^{\text{eff}}\overline{D}_2$, & $\beta_{33}^{\text{eff}}\overline{D}_3 << \beta_{11}^{\text{eff}}\overline{D}_1$). Hence, β_{11}^{eff} can be calculated as:

$$\beta_{11}^{\text{eff}} = \frac{\overline{E}_1}{\overline{D}_1}. \tag{72}$$

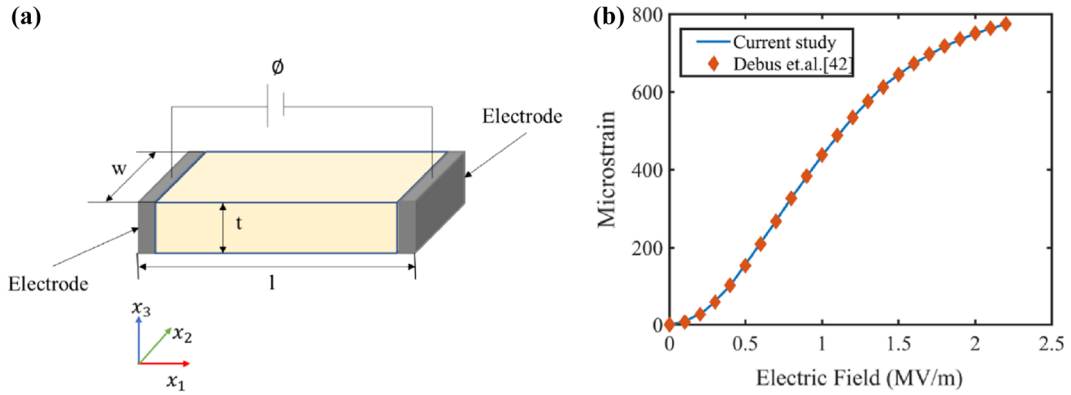

Fig. 4 **a** Geometry of the electrostrictive bar and **b** validation study of induced microstrain as a function of an electric field

Table 2 Constitutive material properties

	$S_{11} = S_{22} = S_{33}$ (m^2/N)	$S_{12} = S_{13} = S_{23}$ (m^2/N)	$S_{44} = S_{55} = S_{66}$ (m^2/N)	Q_{11} (m^4/C^2)	Q_{12} (m^4/C^2)	$b_{11} = b_{33}$ (C/(V.m))	P_s (C/m^2)	k (m/V)
PMN-PT-BT	0.890×10^{-11} [52]	-0.311×10^{-11}	2.4×10^{-11}	0.133×10^{-1} [53]	-0.606×10^{-2}	2.1928×10^{-7} [52]	0.262 [54]	9.20×10^{-7} [52]
Epoxy	2.05×10^{-10} [55]	-7.28×10^{-11}	5.56×10^{-10}	–	–	0.0372×10^{-9} [55]	7.28×10^{-4} [56]	5.11×10^{-8}

Similarly, by applying the analogous boundary conditions as mentioned in Table 1, β_{33}^{eff} can be calculated as:

$$\beta_{33}^{\text{eff}} = \frac{\overline{E}_3}{\overline{D}_3}. \tag{73}$$

3 Results and discussions

For the validation of static finite element formulation, an electrostrictive bar of length l 10 mm, width w, and thickness t of 2 mm is considered, with surface electrodes in the x_1 direction, as shown in Fig. 4.

The material of electrostrictive bar in the validation study is PMN-PT-BT, whose material properties are mentioned in Table 2. Just for validation with Debus et al. [48], the value of Q_{11} is considered as 0.121×10^{-1} m^4/C^2. From Fig. 4b, it is evident that induced microstrain is in good concurrence with the literature; hence, it is prudent to say that the current finite element formulation is validated.

3.1 Mesh sensitivity analysis

After the validation study before evaluating the effective electrostrictive properties of TPMS-based composites, it is wise to perform mesh sensitivity analysis to make sure that the evaluated effective properties are independent of the mesh size. To perform the mesh sensitivity analysis, the TPMS-based electrostrictive composite RVE is discretized using tetrahedral element and effective compliance coefficient S_{11}^{eff} is evaluated for every mesh refinement till the value of effective compliance coefficient S_{11}^{eff} gets saturated. This study is performed for all the TPMS-based structures considered in the current study, i.e., Schoen Gyroid, Neovius, Schoen IWP, and Schwarz primitive, as shown in Fig. 5.

It is necessary to do the convergence study for every TPMS-based composite RVE, as different geometries require different meshes for convergence. For example, the effective compliance coefficient's converged values for the 10% volume fraction of Schoen Gyroid, Neovius, Schoen IWP, and Schwarz primitive-based electrostrictive composites are1.23×10^{-10}, 1.06×10^{-10}, 1.17×10^{-10}, and 1.32×10^{-10} (m^2/N) achieved at 130,636, 167,418, 144,697, and 99,650 number of elements, respectively. After achieving the convergence,

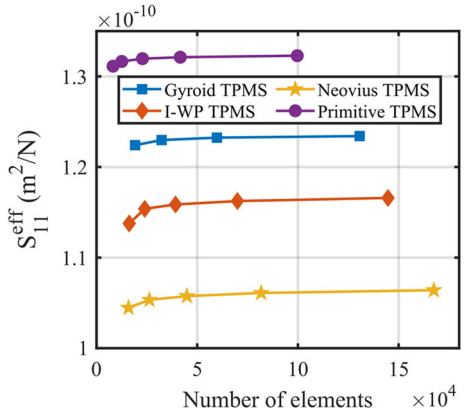

Fig. 5 Mesh sensitivity analysis of effective compliance coefficient S_{11}^{eff} for Schoen Gyroid, Neovius, Schoen IWP, and Schwarz primitive-based electrostrictive composite's RVE

the same mesh refinement is employed for subsequent simulation of effective electrostrictive properties for the corresponding TPMS-based electrostrictive composite. The properties of constitutive materials used in the current study are mentioned in Table 2.

3.2 Effective properties

Ensuring that all the simulation results will be liberated from the mesh size, effective properties can be evaluated. Applying the appropriated boundary conditions mentioned in Table 1, effective electrostrictive properties can be evaluated.

3.2.1 Effective compliance coefficients

All the effective elastic compliance coefficients, i.e., (S_{11}^{eff}, S_{12}^{eff}, S_{33}^{eff}, and S_{66}^{eff}) of Schoen Gyroid, Neovius, Schoen IWP, and Schwarz primitive-based electrostrictive composite, are evaluated simultaneously, as shown in Figs. 6a–d. The volume fraction for every TPMS structure is varied from 10 to 40% with a step size of 5%. For every volume fraction, an RVE was generated as explained in Sect. 2.1. For each TPMS-based electrostrictive composite, seven different RVEs were subjected to boundary conditions employed using the finite element method.

It can be observed from Fig. 6a that the effective compliance coefficient S_{11}^{eff} is decreasing as the volume fraction of TPMS-based structure is increasing, which also satisfies the rule of mixture. As the value of compliance coefficient of epoxy (polymer) is more than PMN-PT-BT (ceramic), the effective compliance coefficient is decreasing with an increase in volume fraction of TPMS structure (PMN-PT-BT). The intuition from the rule of mixture is also justified by all other effective compliance coefficients, i.e., S_{12}^{eff}, S_{33}^{eff}, and S_{66}^{eff} (see Fig. 6b–6d). Not only volume fraction but also the shape of TPMS structure governs the effective properties, which is evident from all Fig. 6a–d. For instance, the value of effective compliance coefficient S_{11}^{eff}, for Schwarz primitive and Schoen Gyroid-based electrostrictive composites, is highest and lowest, respectively, among all the studied structures at 10% volume fraction. The difference in the value of effective compliance coefficient S_{11}^{eff} keeps on reducing as the volume fraction is increasing. However, at a 40% volume fraction, the values of S_{11}^{eff} are almost close, i.e., 4.58×10^{-11}, 3.78×10^{-11}, 3.82×10^{-11}, and 4.92×10^{-11} m^2/N for Schoen Gyroid, Neovius, Schoen IWP, and Schwarz primitive-based electrostrictive composite, respectively. Moreover, this observation holds good for all other effective compliance coefficients (see Fig. 6b–d). The values of all the effective compliance coefficients for all the TPMS-based electrostrictive composite as a function of volume fraction are mentioned in Table 3. However, the values of effectively saturated polarization are calculated from the rule of mixture, and its values for different TPMS composites as a function of volume fraction are mentioned in Table 3.

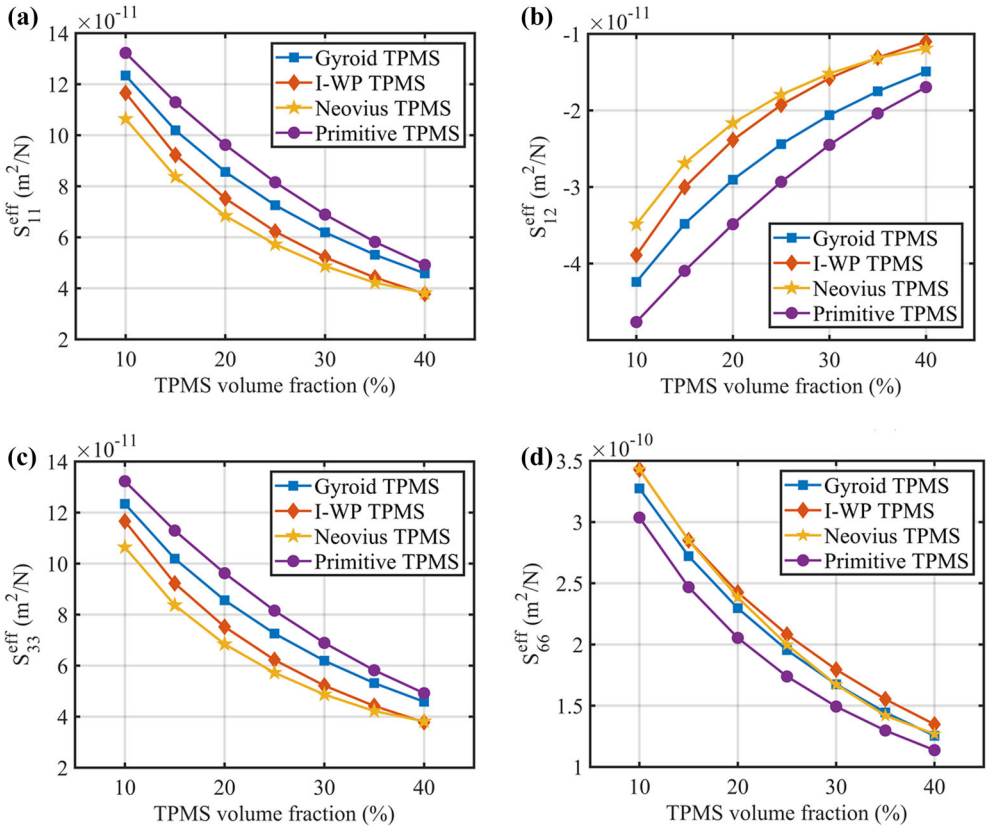

Fig. 6 Variation of effective elastic compliance coefficients **a** S_{11}^{eff}, **b** S_{12}^{eff}, **c** S_{33}^{eff}, and **d** S_{66}^{eff} with TPMS volume fraction

3.2.2 Effective impermeability constant and domain wall constant

The effective impermeability constants (β_{11}^{eff}) and effective domain wall constant k^{eff} for all the different TPMS-based electrostrictive composites as a function of volume fraction are discussed. Effective impermeability constant β_{11}^{eff} decreases as the volume fraction of TPMS increases (see Fig. 7a), and effective domain wall constant also decreases with the increase in volume fraction of TPMS in composite (see Fig. 7b). This decreasing trend justifies the essence of the rule of mixture as both the impermeability constant and domain wall constant of the matrix (epoxy) are more than the reinforcement material (PMN-PT-BT); hence, with an increase in the volume of reinforcement material, the overall effective value decreases. All the values of effective impermeability constant and effective domain wall constant as a function volume fraction of TPMS for Schoen Gyroid, Neovius, Schoen IWP, and Schwarz primitive-based electrostrictive composite are given in Table 4.

3.2.3 Effective electrostrictive coefficients

Effective electrostrictive coefficients for different TPMS-based electrostrictive composites are evaluated as a function of volume fraction using the appropriate boundary conditions mentioned in Table 1. The values of both effective electrostrictive coefficients Q_{11}^{eff}, and Q_{12}^{eff} as a function of volume fraction are depicted in Fig. 8a, b, respectively.

The values of effective electrostrictive coefficient Q_{11}^{eff} are decreasing as the volume fraction is increasing; this trend is justifying the well-known relation $Q \propto \frac{S}{b}$ or $Q \propto \beta S$ (i.e., the electrostrictive coefficient is directly proportional to the compliance coefficient and the impermeability constant) [57]. As it is evident from Figs. 6a and 7a that the effective compliance coefficient and effective impermeability constant are decreasing, it is prudent to say that our results for effective electrostrictive coefficient follow the formerly mentioned relation. All the values of effective electrostrictive coefficients as the function of volume fraction for different TPMS-based composites are given in Table 5.

Table 3 Effective compliance coefficient of TPMS-based electrostrictive composites

Eff. properties	TPMS type	TPMS volume fraction						
		10%	15%	20%	25%	30%	35%	40%
S_{11}^{eff} (m^2/N)	Schoen Gyroid	1.23×10^{-10}	1.02×10^{-10}	8.56×10^{-11}	7.26×10^{-11}	6.19×10^{-11}	5.32×10^{-11}	4.58×10^{-11}
S_{12}^{eff} (m^2/N)		-4.24×10^{-11}	-3.5×10^{-11}	-2.9×10^{-11}	-2.4×10^{-11}	-2.1×10^{-11}	-1.7×10^{-11}	-1.5×10^{-11}
S_{13}^{eff} (m^2/N)		-4.19×10^{-11}	-3.4×10^{-11}	-2.8×10^{-11}	-2.4×10^{-11}	-2×10^{-11}	-1.7×10^{-11}	-1.4×10^{-11}
S_{33}^{eff} (m^2/N)		1.23×10^{-10}	1.02×10^{-10}	8.56×10^{-11}	7.26×10^{-11}	6.19×10^{-11}	5.32×10^{-11}	4.58×10^{-11}
S_{44}^{eff} (m^2/N)		3.27×10^{-10}	2.72×10^{-10}	2.3×10^{-10}	1.95×10^{-10}	1.68×10^{-10}	1.45×10^{-10}	1.25×10^{-10}
S_{66}^{eff} (m^2/N)		3.27×10^{-10}	2.72×10^{-10}	2.3×10^{-10}	1.95×10^{-10}	1.68×10^{-10}	1.45×10^{-10}	1.25×10^{-10}
P_s^{eff} (C/m^2)		0.0268	0.0399	0.0529	0.066	0.0791	0.0921	0.1052
S_{11}^{eff} (m^2/N)	Neovius	1.06×10^{-10}	8.37×10^{-11}	6.84×10^{-11}	5.72×10^{-11}	4.87×10^{-11}	4.22×10^{-11}	3.82×10^{-11}
S_{12}^{eff} (m^2/N)		-3.48×10^{-11}	-2.7×10^{-11}	-2.2×10^{-11}	-1.8×10^{-11}	-1.5×10^{-11}	-1.3×10^{-11}	-1.2×10^{-11}
S_{13}^{eff} (m^2/N)		-3.48×10^{-11}	-2.7×10^{-11}	-2.2×10^{-11}	-1.8×10^{-11}	-1.5×10^{-11}	-1.3×10^{-11}	-1.2×10^{-11}
S_{33}^{eff} (m^2/N)		1.06×10^{-10}	8.37×10^{-11}	6.84×10^{-11}	5.72×10^{-11}	4.87×10^{-11}	4.22×10^{-11}	3.82×10^{-11}
S_{44}^{eff} (m^2/N)		3.43×10^{-10}	2.85×10^{-10}	2.38×10^{-10}	2×10^{-10}	1.67×10^{-10}	1.42×10^{-10}	1.27×10^{-10}
S_{66}^{eff} (m^2/N)		3.43×10^{-10}	2.85×10^{-10}	2.38×10^{-10}	2×10^{-10}	1.67×10^{-10}	1.42×10^{-10}	1.27×10^{-10}
P_s^{eff} (C/m^2)		0.0268	0.0399	0.0529	0.066	0.0791	0.0921	0.1052
S_{11}^{eff} (m^2/N)	Schoen IWP	1.16×10^{-10}	9.23×10^{-11}	7.52×10^{-11}	6.23×10^{-11}	5.22×10^{-11}	4.42×10^{-11}	3.78×10^{-11}
S_{12}^{eff} (m^2/N)		-3.89×10^{-11}	-3×10^{-11}	-2.4×10^{-11}	-1.9×10^{-11}	-1.6×10^{-11}	-1.3×10^{-11}	-1.1×10^{-11}
S_{13}^{eff} (m^2/N)		-3.89×10^{-11}	-3×10^{-11}	-2.4×10^{-11}	-1.9×10^{-11}	-1.6×10^{-11}	-1.3×10^{-11}	-1.1×10^{-11}
S_{33}^{eff} (m^2/N)		1.16×10^{-10}	9.23×10^{-11}	7.52×10^{-11}	6.23×10^{-11}	5.22×10^{-11}	4.42×10^{-11}	3.78×10^{-11}
S_{44}^{eff} (m^2/N)		3.42×10^{-10}	2.85×10^{-10}	2.43×10^{-10}	2.08×10^{-10}	1.8×10^{-10}	1.55×10^{-10}	1.35×10^{-10}
S_{66}^{eff} (m^2/N)		3.42×10^{-10}	2.85×10^{-10}	2.43×10^{-10}	2.08×10^{-10}	1.8×10^{-10}	1.55×10^{-10}	1.35×10^{-10}
P_s^{eff} (C/m^2)		0.0268	0.0399	0.0529	0.066	0.0791	0.0921	0.1052
S_{11}^{eff} (m^2/N)	Schwarz primitive	1.32×10^{-10}	1.13×10^{-10}	9.62×10^{-11}	8.16×10^{-11}	6.89×10^{-11}	5.82×10^{-11}	4.92×10^{-11}
S_{12}^{eff} (m^2/N)		-4.76×10^{-11}	-4.1×10^{-11}	-3.5×10^{-11}	-2.9×10^{-11}	-2.4×10^{-11}	-2×10^{-11}	-1.7×10^{-11}
S_{13}^{eff} (m^2/N)		-4.76×10^{-11}	-4.1×10^{-11}	-3.5×10^{-11}	-2.9×10^{-11}	-2.4×10^{-11}	-2×10^{-11}	-1.7×10^{-11}
S_{33}^{eff} (m^2/N)		1.32×10^{-10}	1.13×10^{-10}	9.62×10^{-11}	8.16×10^{-11}	6.89×10^{-11}	5.82×10^{-11}	4.92×10^{-11}
S_{44}^{eff} (m^2/N)		3.03×10^{-10}	2.47×10^{-10}	2.05×10^{-10}	1.74×10^{-10}	1.49×10^{-10}	1.3×10^{-10}	1.14×10^{-10}
S_{66}^{eff} (m^2/N)		3.03×10^{-10}	2.47×10^{-10}	2.05×10^{-10}	1.74×10^{-10}	1.49×10^{-10}	1.3×10^{-10}	1.14×10^{-10}
P_s^{eff} (C/m^2)		0.0268	0.0399	0.0529	0.066	0.0791	0.0921	0.1052

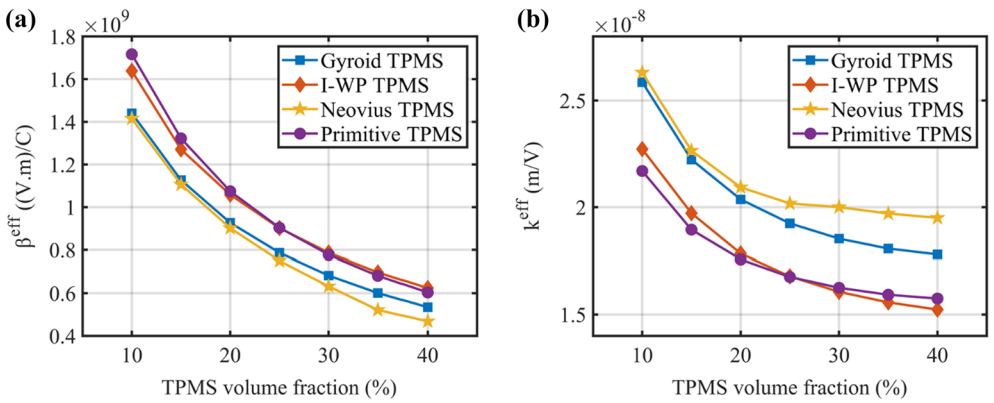

Fig. 7 **a** Effective impermeability constant and **b** effective domain wall constant variation with volume fraction of TPMS

Table 4 Effective impermeability and domain wall constant of TPMS-based electrostrictive composites

Eff. prop	TPMS type	TPMS volume fraction						
		10%	15%	20%	25%	30%	35%	40%
β_{11}^{eff} [(Vm)/C]	Schoen Gyroid	1.44×10^{9}	1.13×10^{9}	9.27×10^{8}	7.87×10^{8}	6.82×10^{8}	6.01×10^{8}	5.34×10^{8}
β_{33}^{eff} [(Vm)/C]		1.44×10^{9}	1.13×10^{9}	9.27×10^{8}	7.87×10^{8}	6.82×10^{8}	6.01×10^{8}	5.34×10^{8}
k^{eff} (m/V)		2.58×10^{-8}	2.22×10^{-8}	2.04×10^{-8}	1.92×10^{-8}	1.85×10^{-8}	1.81×10^{-8}	1.78×10^{-8}
β_{11}^{eff} [(Vm)/C]	Neovius	1.41×10^{9}	1.11×10^{9}	9.02×10^{8}	7.51×10^{8}	6.32×10^{8}	5.21×10^{8}	4.68×10^{8}
β_{33}^{eff} [(Vm)/C]		1.41×10^{9}	1.11×10^{9}	9.02×10^{8}	7.51×10^{8}	6.32×10^{8}	5.21×10^{8}	4.68×10^{8}
k^{eff} (m/V)		2.63×10^{-8}	2.26×10^{-8}	2.09×10^{-8}	2.02×10^{-8}	2×10^{-8}	1.97×10^{-8}	1.95×10^{-8}
β_{11}^{eff} [(Vm)/C]	Schoen IWP	1.63×10^{9}	1.27×10^{9}	1.06×10^{9}	9.02×10^{8}	7.87×10^{8}	6.97×10^{8}	6.24×10^{8}
β_{33}^{eff} [(Vm)/C]		1.63×10^{9}	1.27×10^{9}	1.06×10^{9}	9.02×10^{8}	7.87×10^{8}	6.97×10^{8}	6.24×10^{8}
k^{eff} (m/V)		2.27×10^{-8}	1.97×10^{-8}	1.78×10^{-8}	1.68×10^{-8}	1.61×10^{-8}	1.56×10^{-8}	1.52×10^{-8}
β_{11}^{eff} [(Vm)/C]	Schwarz primitive based	1.71×10^{9}	1.32×10^{9}	1.07×10^{9}	9.04×10^{8}	7.78×10^{8}	6.81×10^{8}	6.03×10^{8}
β_{33}^{eff} [(Vm)/C]		1.71×10^{9}	1.32×10^{9}	1.07×10^{9}	9.04×10^{8}	7.78×10^{8}	6.81×10^{8}	6.03×10^{8}
k^{eff} (m/V)		2.16×10^{-8}	1.89×10^{-8}	1.76×10^{-8}	1.68×10^{-8}	1.63×10^{-8}	1.59×10^{-8}	1.57×10^{-8}

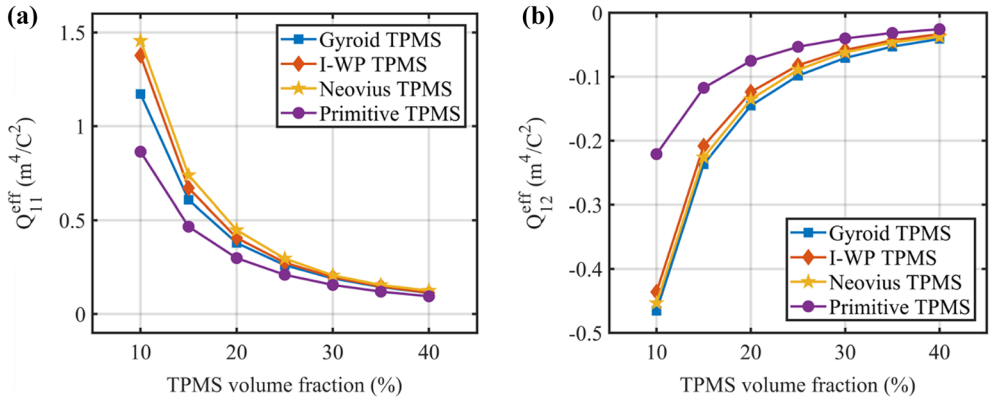

Fig. 8 Electrostrictive coefficients **a** Q_{11}^{eff}, and **b** Q_{12}^{eff} illustrated as a function of volume fraction of different TPMS structures

Table 5 Effective electrostrictive coefficients of TPMS-based composites as a function of volume fraction

Eff. prop	TPMS type	TPMS volume fraction						
		10%	15%	20%	25%	30%	35%	40%
Q_{11}^{eff} (m^4/C^2)	Schoen Gyroid	1.1716	0.6073	0.3792	0.2606	0.1899	0.144	0.1123
Q_{12}^{eff} (m^4/C^2)		−0.465	−0.237	−0.145	−0.098	−0.070	−0.0529	−0.041
Q_{11}^{eff} (m^4/C^2)	Neovius	1.455	0.739	0.447	0.296	0.206	0.154	0.124
Q_{12}^{eff} (m^4/C^2)		−0.453	−0.226	−0.135	−0.089	−0.062	−0.046	−0.037
Q_{11}^{eff} (m^4/C^2)	Schoen IWP	1.377	0.6703	0.4062	0.2741	0.1967	0.1471	0.1132
Q_{12}^{eff} (m^4/C^2)		−0.436	−0.208	−0.123	−0.082	−0.058	−0.043	−0.033
Q_{11}^{eff} (m^4/C^2)	Schwarz primitive based	0.863	0.465	0.298	0.209	0.155	0.119	0.0945
Q_{12}^{eff} (m^4/C^2)		−0.221	−0.117	−0.075	−0.053	−0.040	−0.0315	−0.025

4 Conclusions

A model to predict the homogenized properties of TPMS-based electrostrictive composites, which employs the finite element method is presented in the current study. Finite element formulation is presented to solve the nonlinear electrostrictive constitutive equations. All the results satisfy the intuition from the rule of mixture and relations established in the literature (i.e., $Q \propto \frac{S}{b}$ or $Q \propto \beta S$). The composites consist of epoxy matrix and PMN-PT-BT as TPMS structure reinforcement. The study considered the four different structures, i.e., Schoen Gyroid, Neovius, Schoen IWP, and Schwarz primitive for TPMS-based electrostrictive composite for the present work. Effective properties are not only a function of the volume fraction of reinforcement but also their structures. Even on considering the non-electrostrictive matrix, the TPMS-based electrostrictive composite is showing more value of electrostriction coefficient than the PMN-PT-BT at a 10% volume fraction independent of any TPMS structure. The maximum value of effective electrostrictive coefficient [i.e., $Q_{11}^{\text{eff}} = 1.455\,(\text{m}^4/\text{C}^2)$] is achieved for Neovius electrostrictive composite. It is prudent to say that these composites will find their place in practical application owing to their salient features of more flexibility and high electrostrictive coefficient. From the current study, it is revealed that an even higher electrostrictive coefficient can be achieved if a matrix of electrostrictive active polymer is selected.

Appendix A

Shape function N_i for linear tetrahedral element is

$$N_i = \frac{(\alpha_i + \beta_i x_1 + \gamma_i x_2 + \delta_i x_3)}{6V}, \tag{A.1}$$

where i varies from 1 to 4, and

$$\alpha_1 = \begin{vmatrix} x_1^2 & x_2^2 & x_3^2 \\ x_1^3 & x_2^3 & x_3^3 \\ x_1^4 & x_2^4 & x_3^4 \end{vmatrix}, \beta_1 = -\begin{vmatrix} 1 & x_2^2 & x_3^2 \\ 1 & x_2^3 & x_3^3 \\ 1 & x_2^4 & x_3^4 \end{vmatrix}, \gamma_1 = \begin{vmatrix} 1 & x_1^2 & x_3^2 \\ 1 & x_1^3 & x_3^3 \\ 1 & x_1^4 & x_3^4 \end{vmatrix}, \delta_1 = -\begin{vmatrix} 1 & x_1^2 & x_2^2 \\ 1 & x_1^3 & x_2^3 \\ 1 & x_1^4 & x_2^4 \end{vmatrix}, \tag{A.2}$$

$$\alpha_2 = -\begin{vmatrix} x_1^1 & x_2^1 & x_3^1 \\ x_1^3 & x_2^3 & x_3^3 \\ x_1^4 & x_2^4 & x_3^4 \end{vmatrix}, \beta_2 = \begin{vmatrix} 1 & x_2^1 & x_3^1 \\ 1 & x_2^3 & x_3^3 \\ 1 & x_2^4 & x_3^4 \end{vmatrix}, \gamma_2 = -\begin{vmatrix} 1 & x_1^1 & x_3^1 \\ 1 & x_1^3 & x_3^3 \\ 1 & x_1^4 & x_3^4 \end{vmatrix}, \delta_2 = \begin{vmatrix} 1 & x_1^1 & x_2^1 \\ 1 & x_1^3 & x_2^3 \\ 1 & x_1^4 & x_2^4 \end{vmatrix}, \tag{A.3}$$

$$\alpha_3 = \begin{vmatrix} x_1^1 & x_2^1 & x_3^1 \\ x_1^2 & x_2^2 & x_3^2 \\ x_1^4 & x_2^4 & x_3^4 \end{vmatrix}, \beta_3 = -\begin{vmatrix} 1 & x_2^1 & x_3^1 \\ 1 & x_2^2 & x_3^2 \\ 1 & x_2^4 & x_3^4 \end{vmatrix}, \gamma_3 = \begin{vmatrix} 1 & x_1^1 & x_3^1 \\ 1 & x_1^2 & x_3^2 \\ 1 & x_1^4 & x_3^4 \end{vmatrix}, \delta_3 = -\begin{vmatrix} 1 & x_1^1 & x_2^1 \\ 1 & x_1^2 & x_2^2 \\ 1 & x_1^4 & x_2^4 \end{vmatrix}, \tag{A.4}$$

$$\alpha_4 = -\begin{vmatrix} x_1^1 & x_2^1 & x_3^1 \\ x_1^2 & x_2^2 & x_3^2 \\ x_1^3 & x_2^3 & x_3^3 \end{vmatrix}, \beta_3 = \begin{vmatrix} 1 & x_2^1 & x_3^1 \\ 1 & x_2^2 & x_3^2 \\ 1 & x_2^3 & x_3^3 \end{vmatrix}, \gamma_3 = -\begin{vmatrix} 1 & x_1^1 & x_3^1 \\ 1 & x_1^2 & x_3^2 \\ 1 & x_1^3 & x_3^3 \end{vmatrix}, \delta_3 = \begin{vmatrix} 1 & x_1^1 & x_2^1 \\ 1 & x_1^2 & x_2^2 \\ 1 & x_1^3 & x_2^3 \end{vmatrix}, \tag{A.5}$$

$$6V = \begin{vmatrix} 1 & x_1^1 & x_2^1 & x_3^1 \\ 1 & x_1^2 & x_2^2 & x_3^2 \\ 1 & x_1^3 & x_2^3 & x_3^3 \\ 1 & x_1^4 & x_2^4 & x_3^4 \end{vmatrix}, \tag{A.6}$$

where the superscript (i.e., 1, 2, 3, and 4) represents the node number and the subscript (i.e., 1, 2, and 3) represents the direction.

The elemental strain displacement matrix is

$$[B]_e = \frac{1}{6V}\begin{bmatrix} \beta_1 & 0 & 0 & \beta_2 & 0 & 0 & \beta_3 & 0 & 0 & \beta_4 & 0 & 0 \\ 0 & \gamma_1 & 0 & 0 & \gamma_2 & 0 & 0 & \gamma_3 & 0 & 0 & \gamma_4 & 0 \\ 0 & 0 & \delta_1 & 0 & 0 & \delta_2 & 0 & 0 & \delta_3 & 0 & 0 & \delta_4 \\ 0 & \delta_1 & \gamma_1 & 0 & \delta_2 & \gamma_2 & 0 & \delta_3 & \gamma_3 & 0 & \delta_4 & \gamma_4 \\ \delta_1 & 0 & \beta_1 & \delta_2 & 0 & \beta_2 & \delta_3 & 0 & \beta_3 & \delta_4 & 0 & \beta_4 \\ \gamma_1 & \beta_1 & 0 & \gamma_2 & \beta_2 & 0 & \gamma_3 & \beta_3 & 0 & \gamma_4 & \beta_4 & 0 \end{bmatrix}. \tag{A.7}$$

The elemental electric field and electric potential matrix is

$$\left[B_\phi\right]_e = \begin{bmatrix} \frac{\partial N_1}{\partial x_1} & \frac{\partial N_2}{\partial x_1} & \frac{\partial N_3}{\partial x_1} & \frac{\partial N_4}{\partial x_1} \\ \frac{\partial N_1}{\partial x_2} & \frac{\partial N_2}{\partial x_2} & \frac{\partial N_3}{\partial x_2} & \frac{\partial N_4}{\partial x_2} \\ \frac{\partial N_1}{\partial x_3} & \frac{\partial N_2}{\partial x_3} & \frac{\partial N_3}{\partial x_3} & \frac{\partial N_4}{\partial x_3} \end{bmatrix}. \tag{A.8}$$

References

1. Zhuang, X., Nguyen, C., Nanthakumar, S.S., Chamoin, L., Jin, Y., Rabczuk, T.: Inverse design of reconfigurable piezoelectric topological phononic plates. Mater. Des. **219** 110760 (2022)
2. Mortazavi, B., Shojaei, F., Javvaji, B., Rabczuk, T., Zhuang, X.: Outstandingly high thermal conductivity, elastic modulus, carrier mobility and piezoelectricity in two-dimensional semiconducting CrC2N4: a first-principles study. Mater. Today Energy. **22**, 100839 (2021)
3. Ghasemi, H., Park, H.S., Rabczuk, T.: A multi-material level set-based topology optimization of flexoelectric composites. Comput. Methods Appl. Mech. Eng. **332**, 47–62 (2018)
4. Ghasemi, H., Park, H.S., Zhuang, X., Rabczuk, T.: Three-dimensional isogeometric analysis of flexoelectricity with MATLAB implementation. Comput. Mater. Contin. **65**, 1157–1179 (2020)
5. Hamdia, K.M., Ghasemi, H., Zhuang, X., Rabczuk, T.: Multilevel Monte Carlo method for topology optimization of flexoelectric composites with uncertain material properties. Eng. Anal. Bound. Elem. **134**, 412–418 (2022)
6. Sharma, S., Kumar, R., Talha, M., Vaish, R.: Flexoelectric poling of functionally graded ferroelectric materials. Adv. Theory Simul. **4**, 2000158 (2021)
7. Diguet, G., Cavaille, J.-Y., Sebald, G., Takagi, T., Yabu, H., Suzuki, A., Miura, R.: Physical behavior of electrostrictive polymers. Part 1: Polarization forces. Comput. Mater. Sci. **190**, 110294 (2021)
8. Tohluebaji, N., Thainiramit, P., Putson, C., Muensit, N.: Phase and structure behavior vs. electromechanical performance of electrostrictive P (VDF-HFP)/ZnO composite nanofibers. Polymers (Basel) **13**, 2565 (2021)
9. Farhan, R., Eddiai, A., Meddad, M., Chakhchaoui, N., Rguiti, M., Mazroui, M.: Improvement in energy conversion of electrostrictive composite materials by new approach via piezoelectric effect: modeling and experiments. Polym. Adv. Technol. **32**, 123–130 (2021)
10. Sundar, V., Newnham, R.E.: Electrostriction and polarization. Ferroelectrics **135**, 431–446 (1992)
11. Hom, C.L., Shankar, N.: A fully coupled constitutive model for electrostrictive ceramic materials. J. Intell. Mater. Syst. Struct. **5**, 795–801 (1994)
12. Hom, C.L., Shankar, N.: A finite element method for electrostrictive ceramic devices. Int. J. Solids Struct. **33**, 1757–1779 (1996). https://doi.org/10.1016/0020-7683(95)00123-9
13. Bai, Y., Cheng, Z.-Y., Bharti, V., Xu, H.S., Zhang, Q.M.: High-dielectric-constant ceramic-powder polymer composites. Appl. Phys. Lett. **76**, 3804–3806 (2000)
14. Wang, J.J., Meng, F.Y., Ma, X.Q., Xu, M.X., Chen, L.Q.: Lattice, elastic, polarization, and electrostrictive properties of BaTiO 3 from first-principles. J. Appl. Phys. **108**, 34107 (2010)
15. Tang, T., Yu, W.: Effective nonlinear behavior of electrostrictive multiphase composites: a micromechanical study. Int. J. Eng. Sci. **48**, 1769–1777 (2010)
16. Farhan, R., Eddiai, A., Meddad, M., Mazroui, M., Guyomar, D.: Electromechanical losses evaluation by energy-efficient method using the electrostrictive composites: experiments and modeling. Smart Mater. Struct. **28**, 35024 (2019)
17. Li, J.Y.: The effective electroelastic moduli of textured piezoelectric polycrystalline aggregates. J. Mech. Phys. Solids **48**, 529–552 (2000)
18. Fang, D.-N., Jiang, B., Hwang, K.-C.: A model for predicting effective properties of piezocomposites with non-piezoelectric inclusions. J. Elast. Phys. Sci. Solids. **62**, 95–118 (2001)
19. Sabina, F.J., Rodríguez-Ramos, R., Bravo-Castillero, J., Guinovart-Díaz, R.: Closed-form expressions for the effective coefficients of a fibre-reinforced composite with transversely isotropic constituents. II: Piezoelectric and hexagonal symmetry. J. Mech. Phys. Solids. **49**, 1463–1479 (2001)
20. Aboudi, J.: Micromechanical prediction of the effective coefficients of thermo-piezoelectric multiphase composites. J. Intell. Mater. Syst. Struct. **9**, 713–722 (1998)
21. Castaneda, P.P., Suquet, P.: Nonlinear composites. Adv. Appl. Mech. **34**, 171–302 (1997)
22. Castañeda, P.P.: Exact second-order estimates for the effective mechanical properties of nonlinear composite materials. J. Mech. Phys. Solids. **44**, 827–862 (1996)

23. Willis, J.R.: On methods for bounding the overall properties of nonlinear composites. J. Mech. Phys. Solids **39**, 73–86 (1991)
24. Talbot, D.R.S., Willis, J.R.: Three-point bounds for the overall properties of a nonlinear composite dielectric. IMA J. Appl. Math. **57**, 41–52 (1996)
25. Guillot, F.M., Jarzynski, J., Balizer, E.: Measurement of electrostrictive coefficients of polymer films. J. Acoust. Soc. Am. **110**, 2980–2990 (2001)
26. Li, J., Rao, N.: Micromechanics of ferroelectric polymer-based electrostrictive composites. J. Mech. Phys. Solids **52**, 591–615 (2004)
27. Lebrun, L., Guyomar, D., Guiffard, B., Cottinet, P.-J., Putson, C.: The Characterisation of the harvesting capabilities of an electrostrictive polymer composite. Sens Actuators A Phys. **153**, 251–257 (2009)
28. Li, S., Xiong, D., Liu, M., Bai, S., Zhao, X.: Thermophysical properties of SiC/Al composites with three dimensional interpenetrating network structure. Ceram. Int. **40**, 7539–7544 (2014)
29. Cheng, F., Kim, S.-M., Reddy, J.N., Al-Rub, R.K.A.: Modeling of elastoplastic behavior of stainless-steel/bronze interpenetrating phase composites with damage evolution. Int. J. Plast. **61**, 94–111 (2014)
30. Poniznik, Z., Salit, V., Basista, M., Gross, D.: Effective elastic properties of interpenetrating phase composites. Comput. Mater. Sci. **44**, 813–820 (2008)
31. Al-Ketan, O., Abu Al-Rub, R.K.: Multifunctional mechanical metamaterials based on triply periodic minimal surface lattices. Adv. Eng. Mater. **21**, 1900524 (2019)
32. Al-Ketan, O., Lee, D.-W., Rowshan, R., Al-Rub, R.K.A.: Functionally graded and multi-morphology sheet TPMS lattices: design, manufacturing, and mechanical properties. J. Mech. Behav. Biomed. Mater. **102**, 103520 (2020)
33. Yang, N., Quan, Z., Zhang, D., Tian, Y.: Multi-morphology transition hybridization CAD design of minimal surface porous structures for use in tissue engineering. Comput. Des. **56**, 11–21 (2014)
34. Yang, N., Du, C., Wang, S., Yang, Y., Zhang, C.: Mathematically defined gradient porous materials. Mater. Lett. **173**, 136–140 (2016)
35. Yin, H., Liu, Z., Dai, J., Wen, G., Zhang, C.: Crushing behavior and optimization of sheet-based 3D periodic cellular structures. Compos. Part B Eng. **182**, 107565 (2020)
36. Abueidda, D.W., Dalaq, A.S., Al-Rub, R.K.A., Younes, H.A.: Finite element predictions of effective multifunctional properties of interpenetrating phase composites with novel triply periodic solid shell architectured reinforcements. Int. J. Mech. Sci. **92**, 80–89 (2015)
37. Dalaq, A.S., Abueidda, D.W., Al-Rub, R.K.A., Jasiuk, I.M.: Finite element prediction of effective elastic properties of interpenetrating phase composites with architectured 3D sheet reinforcements. Int. J. Solids Struct. **83**, 169–182 (2016)
38. Dalaq, A.S., Abueidda, D.W., Al-Rub, R.K.A.: Mechanical properties of 3D printed interpenetrating phase composites with novel architectured 3D solid-sheet reinforcements. Compos. Part A Appl. Sci. Manuf. **84**, 266–280 (2016)
39. Al-Rub, R.K.A., Abueidda, D.W., Dalaq, A.S.: Thermo-electro-mechanical properties of interpenetrating phase composites with periodic architectured reinforcements. In: From Creep Damage Mechanics to Homogenization Methods, pp. 1–18. Springer (2015)
40. Wang, L., Lau, J., Thomas, E.L., Boyce, M.C.: Co-continuous composite materials for stiffness, strength, and energy dissipation. Adv. Mater. **23**, 1524–1529 (2011)
41. Abueidda, D.W., Dalaq, A.S., Al-Rub, R.K.A., Jasiuk, I.: Micromechanical finite element predictions of a reduced coefficient of thermal expansion for 3D periodic architectured interpenetrating phase composites. Compos. Struct. **133**, 85–97 (2015)
42. Abueidda, D.W., Al-Rub, R.K.A., Dalaq, A.S., Younes, H.A., Al Ghaferi, A.A., Shah, T.K.: Electrical conductivity of 3D periodic architectured interpenetrating phase composites with carbon nanostructured-epoxy reinforcements. Compos. Sci. Technol. **118**, 127–134 (2015)
43. Abueidda, D.W., Al-Rub, R.K.A., Dalaq, A.S., Lee, D.-W., Khan, K.A., Jasiuk, I.: Effective conductivities and elastic moduli of novel foams with triply periodic minimal surfaces. Mech. Mater. **95**, 102–115 (2016)
44. Gandy, P.J.F., Bardhan, S., Mackay, A.L., Klinowski, J.: Nodal surface approximations to the P, G, D and I-WP triply periodic minimal surfaces. Chem. Phys. Lett. **336**, 187–195 (2001)
45. Brakke, K.A.: The surface evolver. Exp. Math. **1**, 141–165 (1992)
46. Novak, N., Al-Ketan, O., Krstulović-Opara, L., Rowshan, R., Al-Rub, R.K.A., Vesenjak, M., Ren, Z.: Quasi-static and dynamic compressive behaviour of sheet TPMS cellular structures. Compos. Struct. **266**, 113801 (2021)
47. Xu, H., Xie, Y.M., Chan, R., Zhou, S.: Piezoelectric properties of triply periodic minimum surface structures. Compos. Sci. Technol. **200**, 108417 (2020)
48. Debus, J.-C., Dubus, B., Coutte, J.: Finite element modeling of lead magnesium niobate electrostrictive materials: static analysis. J. Acoust. Soc. Am. **103**, 3336–3343 (1998)
49. Devonshire, A.F.: Theory of ferroelectrics. Adv. Phys. **3**, 85–130 (1954)
50. Suo, Z.: Mechanics concepts for failure in ferroelectric ceramics. Smart Struct. Mater. **112**, 1–6 (1991)
51. Suquet, P.: Elements of homogenization theory for inelastic solid mechanics. In: Sanchez-Palencia, E., Zaoui, A. (eds.) Homogenization Techniques for Composite Media, pp. 194–278 (1987)
52. Powers, J.M., McLaughlin, E.A., Moffett, M.B.: PMN measurements at NUWC. NUWC Report, 918 (1995)
53. Hom, C.L., Pilgrim, S.M., Shankar, N., Bridger, K., Massuda, M., Winzer, S.R.: Calculation of quasi-static electromechanical coupling coefficients for electrostrictive ceramic materials. IEEE Trans. Ultrason. Ferroelectr. Freq. Control. **41**, 542–551 (1994)
54. McLaughlin, E.A., Powers, J.M., Moffett, M.B., Janus, R.S.: Characterization of PMN-PT-La for use in high-power electrostrictive projectors. **100**, 2729 (1996)
55. Berger, H., Kari, S., Gabbert, U., Rodriguez-Ramos, R., Bravo-Castillero, J., Guinovart-Diaz, R., Sabina, F.J., Maugin, G.A.: Unit cell models of piezoelectric fiber composites for numerical and analytical calculation of effective properties. Smart Mater. Struct. **15**, 451 (2006)
56. Van den Ende, D.A., Bory, B.F., Groen, W.A., Van Der Zwaag, S.: Properties of quasi 1–3 piezoelectric PZT-epoxy composites obtained by dielectrophoresis. Integr. Ferroelectr. **114**, 108–118 (2010)

57. Eury, S., Yimnirun, R., Sundar, V., Moses, P.J., Jang, S.-J., Newnham, R.E.: Converse electrostriction in polymers and composites. Mater. Chem. Phys. **61**, 18–23 (1999)

Publisher's Note Springer Nature remains neutral with regard to jurisdictional claims in published maps and institutional affiliations.

Springer Nature or its licensor (e.g. a society or other partner) holds exclusive rights to this article under a publishing agreement with the author(s) or other rightsholder(s); author self-archiving of the accepted manuscript version of this article is solely governed by the terms of such publishing agreement and applicable law.